electronics

MDPI

Review

State-of-the-Art Optical Devices for Biomedical Sensing Applications—A Review

N. L. Kazanskiy [1,2], S. N. Khonina [1,2], M. A. Butt [1,3,*], A. Kaźmierczak [3] and R. Piramidowicz [3]

[1] Samara National Research University, 443086 Samara, Russia; kazanskiy@ipsiras.ru (N.L.K.); khonina@ipsiras.ru (S.N.K.)
[2] Institute of RAS-Branch of the FSRC "Crystallography and Photonics" RAS, 443001 Samara, Russia
[3] Institute of Microelectronics and Optoelectronics, Warsaw University of Technology, Koszykowa 75, 00-662 Warsaw, Poland; andrzej.kazmierczak@pw.edu.pl (A.K.); ryszard.piramidowicz@pw.edu.pl (R.P.)
* Correspondence: butt.m@ssau.ru

Abstract: Optical sensors for biomedical applications have gained prominence in recent decades due to their compact size, high sensitivity, reliability, portability, and low cost. In this review, we summarized and discussed a few selected techniques and corresponding technological platforms enabling the manufacturing of optical biomedical sensors of different types. We discussed integrated optical biosensors, vertical grating couplers, plasmonic sensors, surface plasmon resonance optical fiber biosensors, and metasurface biosensors, Photonic crystal-based biosensors, thin metal films biosensors, and fiber Bragg grating biosensors as the most representative cases. All of these might enable the identification of symptoms of deadly illnesses in their early stages; thus, potentially saving a patient's life. The aim of this paper was not to render a definitive judgment in favor of one sensor technology over another. We presented the pros and cons of all the major sensor systems enabling the readers to choose the solution tailored to their needs and demands.

Keywords: surface plasmon resonance; surface plasmon polariton; biomedical applications; refractive index sensing; optical fiber biosensors

Citation: Kazanskiy, N.L.; Khonina, S.N.; Butt, M.A.; Kaźmierczak, A.; Piramidowicz, R. State-of-the-Art Optical Devices for Biomedical Sensing Applications—A Review. *Electronics* **2021**, *10*, 973. https://doi.org/10.3390/electronics10080973

Academic Editors: Woo June Choi and Jun Ki Kim

Received: 23 March 2021
Accepted: 16 April 2021
Published: 19 April 2021

1. Introduction

The design and development of functional biosensors are one of the ways to meet the rising need for highly reliable and successful medical analytical tools. According to the recent report released by Global Market Insights, the global biosensors market is projected to hit USD 42 billion by 2027 [1]. Biosensors are expected to see significant growth in demand over the next six years due to their ability to resolve numerous analytical issues in diverse areas such as medicine, pharmaceutical industry, food safety, and environment protection, among others [2–4]. During the forecast period, the overall biosensors market is projected to be driven by the rising demand for unique detection techniques for early diagnosis in the healthcare field. Furthermore, the growing importance of biosensors in the real world has prompted an increase in R&D activities around the world [5]. Since Clark demonstrated the original idea of an oxygen electrode biosensor in 1956 [6], and ever since then, scientists have made significant advances in biosensing methods, which have since been implemented in clinical practice. For optical measurements, several techniques have been effective, including absorption [7], fluorescence [8], refractometry [9], and polarimetry [10]. Many optical biosensors use evanescent field detection as their primary detection concept [11,12]. Because of their extraordinary response to the change in the regional refractive index (RI) in the vicinity of WG, evanescent field biosensors have drawn growing attention for instantaneous and label-free biomolecular recognition [13].

In cancer studies, biosensors are utilized to evaluate modifications in cell protein content [14]. Cancer cells consume the body's calories and change the mechanism of energy produced by the food in the body, and transmit impulses to surrounding organs, nerves,

and blood vessels, among other things, as they multiply. Human fluids, for instance, blood, tears, saliva, and urine, can be treated as analytes in biomedical care, with various components of the chosen analytes being analyzed [15]. A good example is monitoring the glucose levels, typically connected with the necessity of taking a blood sample and resulting in an obvious discomfort of the patients, while tears may be utilized as an alternative analyte also reflecting the glucose concentration in the blood [16]. Each illness has a higher possibility of being cured when identified sufficiently early. Traditional disease detection methods are time-consuming and are, in most cases, expensive. Modern biosensors are more efficient, of comparable reliability, and typically offer higher detection speeds than many standard techniques, according to researchers [17,18]. Nano- or microfabrication technologies might be deployed to manufacturing such biosensors, enabling utilizing several optical, electrical, and mechanical transducers in these biosensors with simultaneous mitigation of the manufacturing costs. Figure 1 shows the most important of these groupings along with the market demand for biosensors in the present time and forthcoming years.

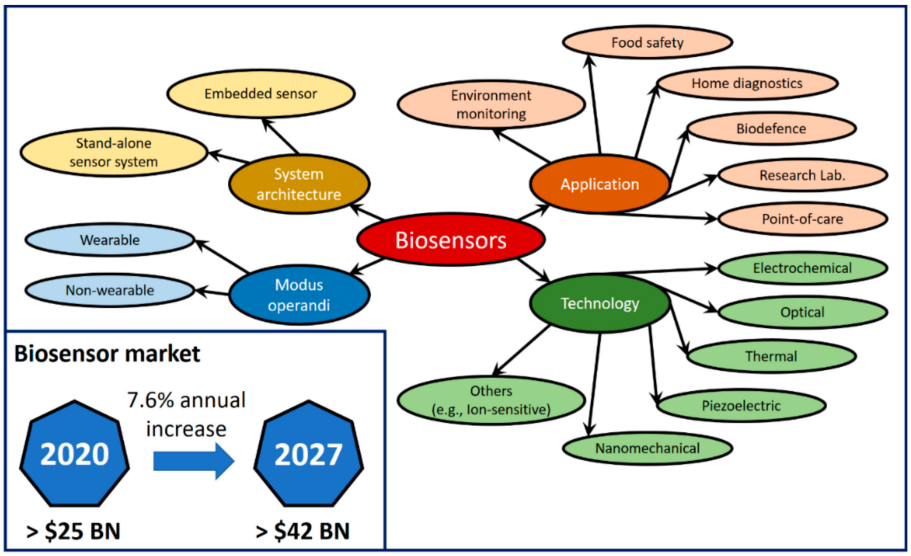

Figure 1. Biosensor's insight and market.

The review paper was structured in the following way. In Section 2, biosensors based on silicon (Si) photonics were discussed. The field of sensing is quite vast, and thus several approaches could be employed. However, in this section, we focused on three main and widely investigated biosensor structures like the Mach–Zehnder interferometer, Young's interferometer, μ-ring resonators, and vertical grating couplers. The next section was devoted to the surface plasmon resonance (SPR) technique, based on the propagation of the SPs at the metal-dielectric boundary, which was exceedingly susceptible to the changes in the RI of the surrounding medium; thus, enabling the implementation of compact and highly sensitive optical fiber biosensors. In this section, the latest advances in SPR-optical fiber-based biomedical devices were discussed. In Section 4, surface plasmon polariton (SPP) based metal-insulator-metal (MIM) WG sensors were discussed, which were widely investigated for the RI sensing application. These sensors are considered highly attractive because of their tiny footprint and elevated sensitivity. Dielectric metasurfaces increased in popularity as a medium for developing new optical biosensors. They revealed many attractive optical properties, involving sharp resonances, strong near-field improvements, and the intriguing ability to retain magnetic modes, owing to their minimal optical loss and intense light-matter association. Section 5 presented the recent advances in these powerful biosensor structures. In Section 6, biosensor designs based on photonic crystals were discussed, followed by thin metal film structures used for biosensing applications presented in Section 7. Section 8 was devoted to biosensors based on optical fiber Bragg

grating structures, which offered extraordinary sensitivity. The paper ended with a brief conclusion presented in Section 9.

2. Integrated Photonic Biosensing Platform

In this segment, we have reviewed the three most commonly studied integrated photonic biosensors based on Mach–Zehnder interferometer (MZI) [19], Young's interferometer (YI) [20], and micro-ring resonator (RRs) [21,22] structures.

2.1. MZI and Young's Interferometer Biomedical Devices

Interferometer-based biomedical sensors are one of the best responsive compact optical devices since they combine two highly sensitive methods: waveguiding and interferometry techniques. A Y-junction divides the propagating light into two single-mode WG paths in a standard interferometric biosensor, one of which contains the sample and is referred to as a sensing arm, while the other is referred to as a reference arm. The sensing arm's evanescent field interacts with the sample and detects a RI variation at the surface, triggering an optical phase change. The beams recombine, after propagating a certain length, resulting in constructive or destructive interference at the output, with the intensity modulation corresponding to the RI change between the sample and reference arm.

Heideman et al. published the first biosensing application utilizing integrated MZIs in the early 1990 s [23]. Ever since, a major advancement has been made in the manufacturing of MZI sensors. Various structures have been successfully developed using a range of fabrication materials, like Si_3N_4 [24], TiO_2 [25], Si [26], and polymers [27] with a detection limit (DL) of 10–^{6} to 10^{-7} RIU. Alternatively, chip-incorporated Young's interferometers (YIs) demonstrated the aptitude to detect biomolecules, resulting in a DL that was comparable to the MZI sensor [28]. In a continuation study in 2000, Brandenburg et al. used Si oxynitride as WGs to reduce the DL of YI sensors to 9×10^{-8} RIU [29]. Schmitt et al. reported Ta_2O_5-based YIs to further boost sensing capacity with the lowest possible DL of 9×10^{-9} RIU [30]. Polymeric materials have also been used in YI sensors in recent years, providing a low-cost, mass-production-ready process with acceptable sensitivity [31].

An exceedingly receptive label-free MZI biosensor created on Si nitride slot WG was demonstrated [24]. The sensing arm of the MZI structure was made of a slot WG, whereas the reference arm was made of a standard ridge WG, unlike typical MZI sensors. Higher sensitivity could be obtained utilizing the slot WG as a sensing region due to the slot WG's property of providing strong optical intensity in the low RI slot region, enabling high light-matter interaction. With a 7 mm long slot WG sensing arm, the bulk RI sensitivity of the slot WG MZI sensor was obtained at 1864/RIU, which is higher than the traditional MZI sensor based on the Si nitride platform. The biotin-streptavidin binding was used to investigate the biosensing capability of the newly formed slot WG MZI. The system's sensitivity was proven to be as small as 18.9 fM or 1 pg/mL of the streptavidin solution [24]. The schematic of the proposed MZI biosensor is shown in Figure 2a, whereas the microscopic image of the fabricated sample is given in Figure 2b [24].

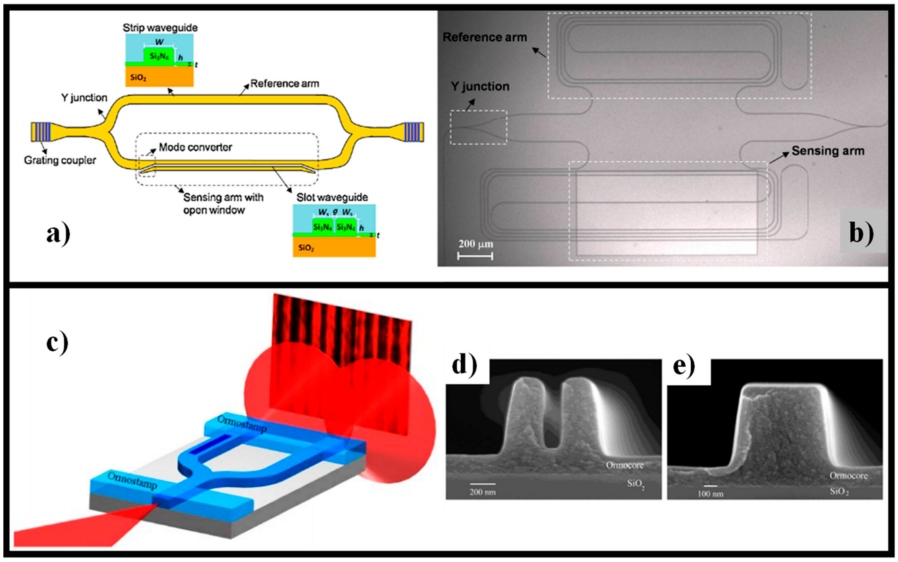

Figure 2. Biosensors based on slot WG configuration: (**a**) graphical representation of the slot-WG-based Mach–Zehnder interferometer (MZI) biosensor consisting of a reference arm and a sensing arm joined with two Y-junctions. Reprinted with permission from ref. [24]; (**b**) microscopic image of the fabricated MZI biosensor. Reprinted with permission from ref. [24]; (**c**) graphical illustration of the slot YI and the measurement setup; (**d**) SEM picture of the cross-section of the slot WG. Reprinted from ref. [32]; (**e**) SEM picture of the cross-section of the reference ridge WG. Reprinted from ref. [32].

In [32], a RI sensor based on the slot WG YI was reported. The interferometer, which works at a visible wavelength of 633 nm, was built on a polymer platform. The phase shift of the interference model was determined using both TE (transverse electric) and TM (transverse magnetic) polarization states with varying concentrations of glucose-water solutions. A RI difference of 6.4×10^{-6} RIU was detected by the sensor in an experiment. Moreover, it was revealed that the slot YI compensated for temperature fluctuations. The findings showed that a polymer slot YI, which could be manufactured using a simple molding process, could provide high-performance sensing capability. The graphical illustration of the principle of the slot YI is displayed in Figure 2c, and the SEM pictures of the manufactured device are displayed in Figure 2d,e [32].

2.2. Silicon µ-RR Biosensors

Si photonic sensors have been extensively explored to be employed in important areas like fundamental medical research and diagnosis, bioterrorism detection, smart home healthcare diagnostics, and gas detecting [33–35]. High sensitivity is desired in these devices, which robustly relies on device size, optical loss, light polarization, and light-matter interaction. Nonetheless, these performance values may not all be improved instantaneously; there is constantly a compromise. Consequently, there is a demand to construct such devices, which are low-cost and straightforward to implement, based on currently available technology. Optical RRs have gained a lot of interest in the latest years as one of the most promising biological sensors [36,37]. This type of sensor assesses variations in light behavior by the interaction of an EM wave with biological molecules such as proteins, bacteria, cells, or DNA samples to determine the target molecules [38]. An interesting review on label-free biochemical sensing utilizing whispering gallery mode optical RRs was presented in [39]. The contact between the evanescent field and the bioparticles in the enveloping medium caused the change of light behavior. The presence of bioparticles in the medium altered the effective refractive index of the medium, causing a deviation in the resonator's resonance conditions. The resonance wavelength deviation of the resonator, which is associated with the number of bioparticles in the medium,

was a product of such an interaction. An active polymer layer could be deposited on the top to enable the resonator's periphery to absorb bioparticles. This layer could mechanically absorb or chemically react with the target bioparticles, causing a change in the effective index of the resonating mode [40].

In recent times, several eye-catching RR schemes have been demonstrated for lab-on-chip biosensing applications. The sensitivity of RRs that is $\Delta\lambda$/RIU depends on the degree of contact of the evanescent field with the analytes. The major portion of the optical power propagated in the high index WG core in the strip WG design, while only a minor portion traveled in the sample. The light-matter interaction could be enhanced by employing slot WGs. A slot-WG is made up of two high-index rails isolated by a subwavelength wide low index slot area [41]. With appropriate configuration, this double core arrangement functions as a single WG, supporting only the lowest order TE and TM modes, with a substantial portion of the electric field of the TE mode transmitting in the low index slot. In [42], an array of optical slot-WG RR sensors, combined with microfluidic sample managing in a miniature unit, for multiplexed label-free biosensing was proposed, as shown in Figure 3a. The elevated sensitivity of the slot-WG RRs merged with on-chip referencing, and physical modeling offered a volume RI DL of 5×10^{-6} RIU and a surface mass density DL of 0.9 pg/mm^2 [43]. Subwavelength grating (SWG) WGs were highly desirable as they could tailor the effective index and dispersion characteristics of the driven mode. SWG WG-based RRs were highly sensitive due to the enhanced light-matter interaction [40,41,44,45]. In [46], a 30 µm diameter SWG RR was realized for biosensing applications. It offered a high sensitivity of 490 nm/RIU and a device DL of 2×10^{-6} RIU. The SEM picture of the fabricated RR is displayed in Figure 3b along with a magnified image of a segment, which is shown in the inset of the figure. Several interesting results were obtained by employing a double SWG WG RR configuration [44]. A non-contact piezoelectric (inkjet) method for the quick and effective printing of bioactive proteins, glycoproteins, and neoglycoconjugates onto a high-density Si µ-RR biosensor array was demonstrated as shown in Figure 3c [47]. This method proved the accessible manufacture of multiplexed Si photonic biomedical sensors for lab-on-a-chip functions and was additionally related to the functionalization of any semiconductor-based biomedical sensor chip [47]. A brightfield micrograph displaying an array of Si photonic RR biosensors is presented in Figure 3d. Further, the SEM image of a range of three exposed µ-rings and one temperature reference µ-ring is revealed in Figure 3e. Electrical thermo-optic tuning of ultrahigh-Q µ-toroid resonators was demonstrated and proposed for biomedical applications [48]. The SEM picture of the RR is exhibited in Figure 3f.

2.3. Vertical Grating Coupler (VGC)

Vertical grating coupler (VGC) is a photonic device that is formed by a finite number of periodic perturbations of the WG height of a shape chosen appropriately to vertically in- and out-couple optical signals to/from WGs via chip facet. In its conventional form, well-known from SOI- [49] and SiN- [50] integrated photonics technologies, VGCs are deeply patterned (i.e., having a perturbation depth like the WG height) structures and offer large coupling angle tolerances and wide 1dB bandwidth (typical values of 40 nm in the case of SOI gratings). This type of VGCs can be used as an efficient coupling structure between integrated photonic WGs and optical fibers or free-space optical components as well as in vertical chip-to-chip optical signal coupling. Although the operation of such grating depends on the effective refractive index of the mode guided in the patterned WG (affected by the ambient), the wide bandwidth of this type of grating prevents it to serve as a sensor.

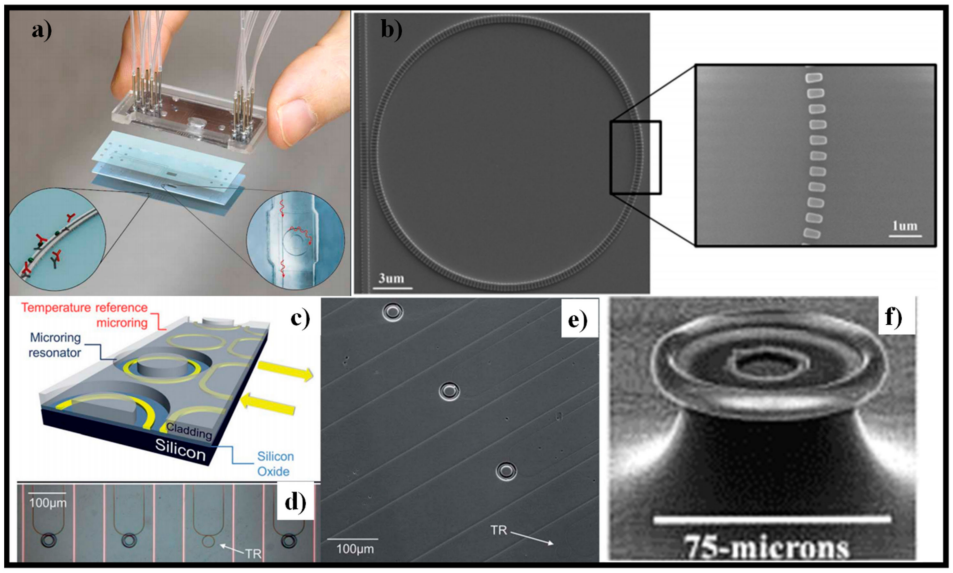

Figure 3. Different micro-ring resonator (RR) designs: (**a**) a packaged optical slot-WG RR sensor array for multiplex label-free assays in labs-on-chips. Reprinted from ref. [42]; (**b**) sub-wavelength grating for enhanced RR biosensor. Reprinted from ref. [46]; (**c**) three-dimensional (3D) graphical illustration of several adjacent devices on a Si photonic µ-RR biosensor array. Reprinted with permission from ref. [47]; (**d**) a brightfield micrograph showing an array of Si photonic µ-RR biosensors. Reprinted with permission from ref. [47]; (**e**) SEM image showing an array of three exposed µ-rings and one temperature reference µ-ring. Reprinted with permission from ref. [47]; (**f**) microtoroid resonator. Reprinted with permission from ref. [48].

On the contrary, the shallowly patterned gratings, especially when fabricated in sol-gel-derived WG films, seem to be a very attractive candidate for being used as a photonic sensor device. Such VGCs were reported in this application for the first time by Lukosz et al. [51,52]. The research groups, led by Szendrö, also significantly contributed to the development of this topic [53,54], leading to the commercial implementation of this device [55]. VGCs sensors were also developed by the group led by Karasiński [56–58] and by several other researchers [59–63]. The operation of such a sensor is depicted schematically in Figure 4. Inspired by [58].

The quasi-parallel light beam was inserted from the bottom to the VGC structure, and, in the case of the optimal coupling angle, it was coupled to the WG layer. The optimal coupling angle Θ depended on the effective refractive index of the guided mode in the WG layer that was affected by the material indices of the substrate (n_S), WG film (n_W), and the ambient above the grating (n_A). Typically, VGCs sensors were read out in a goniometric setup using a fixed-wavelength laser source, where the optimal coupling angle varied with the fluctuation of the refractive index change of the measured material above the grating. An exemplary schematic of such a setup is shown in Figure 5 [57].

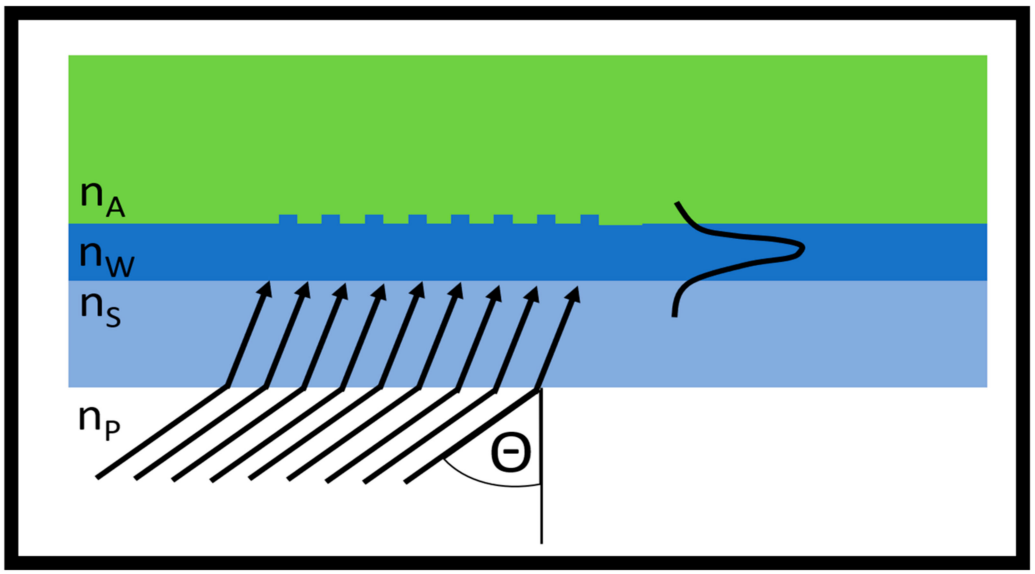

Figure 4. Schematic operation of a vertical grating coupler (VGC)-based sensor. Adapted from ref. [57].

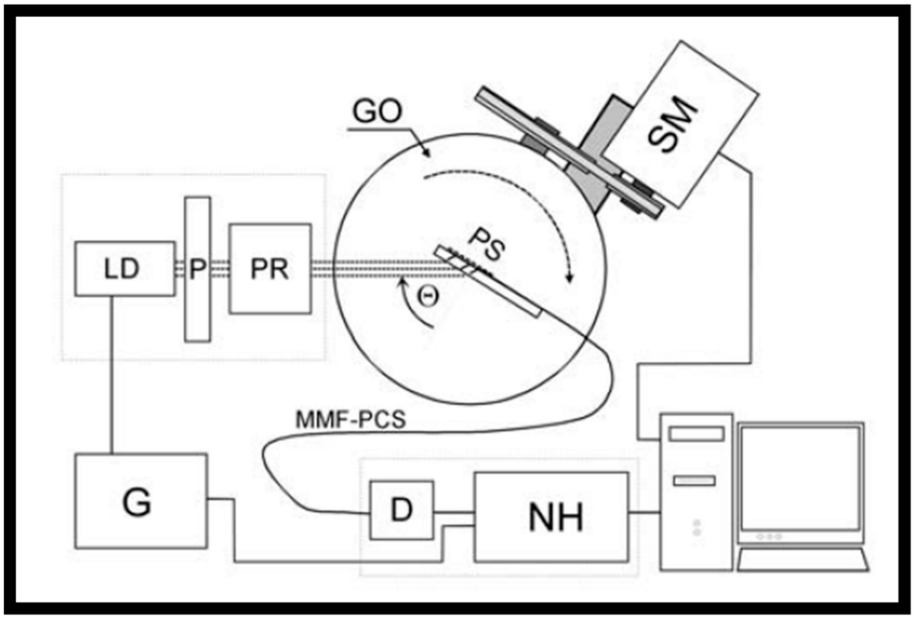

Figure 5. Schematics of the measurement setup for VGC sensors. Reprinted from ref. [57]. PS—planar structure, GO—goniometer, SM—stepping motor, LD—laser diode, P—polarizer, PR—polarizer rotator, G—generator, D—detector, NH—homodyne nanovoltmeter.

The shallow pattern of the sensor VGC resulted in a tight in-coupling resonance condition; this was not very profitable for the input coupler efficiency (that was not an issue in the case of the sensor device) but made the readout of the exact optimal coupling angle more precise. An example of the angular modal spectra of the SiO_2:TiO_2 VGC taken from [58] is shown in Figure 6.

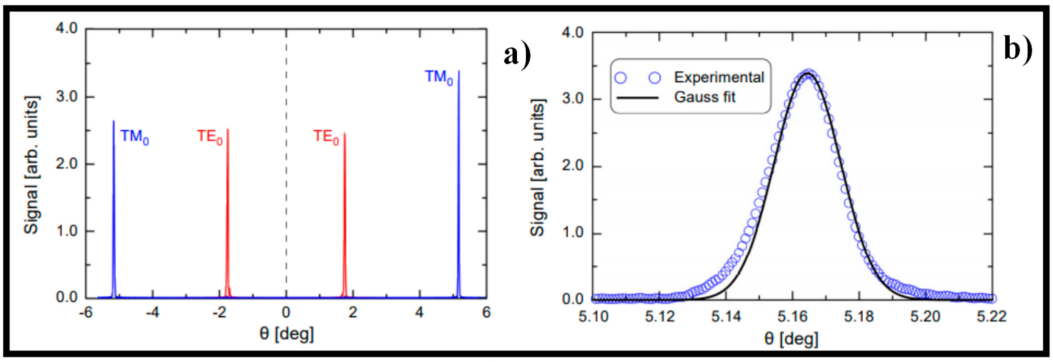

Figure 6. Angle modal spectra of the surface grating coupler used in the experiment (**a**) and a close-up on the in-coupling peak TM0 (full width at half-maximum (FWHM) = 0.024°); (**b**) Reprinted from ref. [58].

Consequently, the VGC sensors fabricated in SiO_2-TiO_2 WG films demonstrated a high sensitivity of about 16°/RIU with a detection limit for ambient refractive index sensing as low as 5.0×10^{-6} RIU [56]. One of the fundamental advantages of VGC sensors is their fabrication simplicity. Typically, VGC-based sensor devices are fabricated on glass substrates in sol-gel-derived titanium oxide (TiO_2) based or polymer WG films. Fabrication of such a sensor device starts with the WG film deposition using a spin or dip-coating technique. Further, the grating pattern is directly imprinted on the non-hardened WG film. Finally, the WG film is hardened. No additional expensive technological steps such as lithography or etching are required for the fabrication of such sensor structures. This process is schematically shown in Figure 7.

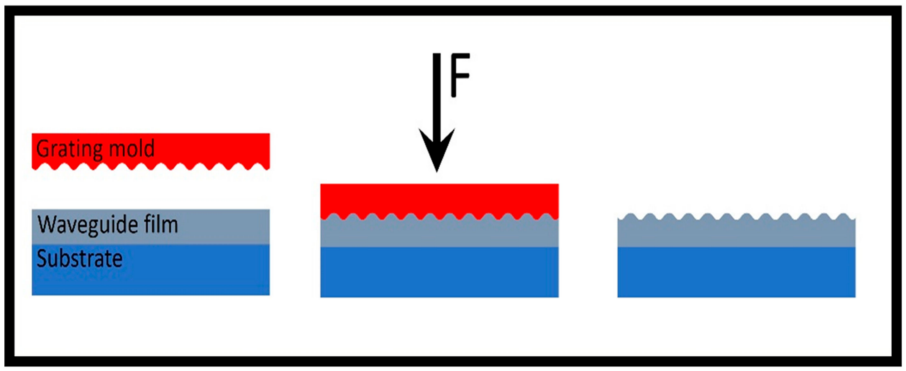

Figure 7. Schematic representation of VGC sensor fabrication by direct imprinting on WG film.

The possibility of multichannel operations of such sensor devices leading to prospective multiparameter sensing was highlighted in [58]. Additionally, in this case, the sensor device fabrication was limited to imprinting a single grating coupler on the WG film.

3. SPR-Optical Fiber-Based Biosensors

Localized surface plasmon resonance (LSPR) and propagating surface plasmon polaritons (SPPs) are two categories of SPR [64]. When the size of a metallic nanostructure is smaller than the incident wavelength of light, LSPR occurs, resulting in collective but non-propagating oscillations of the surface electrons in the metallic nanostructure [65]. The LSPR is considerably affected by the RI of the surrounding medium, making colorimetric plasmonic sensors possible [66,67]. The incident EM field is also concentrated around the nanostructure by LSPR. Plasmon-enhanced fluorescence (PEF) [68,69], surface-enhanced Raman scattering (SERS) [70,71], and surface-enhanced infrared absorption spectroscopy (SEIAS) [72,73] are all examples of how the local EM field can affect optical effects like fluorescence, Raman scattering, and infrared absorption. The LSPR-related EM field stretches into the ambient medium (usually 30 nm) and deteriorates exponentially for a dipole.

SPPs, in distinction to LSPR, are charge oscillations circulating on the surface of thin metal films. SPP cannot be excited by free-space radiations; as an alternative, resonance excitation requires momentum matching, for instance, by periodicity in a nanostructure. The RI of the ambient medium modulates SPP, which then transduces the sensor's signal. In PEF and SERS, SPP can also be used to modulate radiation. The evanescent EM field of SPP decomposes with a longer length (usually 200 nm) than that of LSPR, permitting the SPP to be modulated by modification at a distance greater than that of LSPR. For label-free biomolecule identification, SPP modes were utilized in sensing applications. Since SPP propagated hundreds of μm along the surface, it varied from LSPR for sensing. This had a unique benefit in that the incident laser could prevent physical contact with the sample under observation. This prevented interference from heavy background noise as well as disruption to the sample from the high-energy laser [74].

SPR-based optical fibers operate on the theory of the guided EM wave [75]. The biggest portion of the EM-wave propagates through the core of the optical fiber, but a minor fraction of it extends from the cladding as an evanescent field, which collides with the plasmonic metal surface, and excites the free electrons [76]. When the frequency of the incident photon and the free electrons are complemented, the electrons begin to vibrate, and an SP wave is formed at the metal-dielectric boundary. At the resonance state, a sharp loss peak occurs, which is highly responsive to the RI of the ambient medium. SPR sensors based on optical fibers were first commercialized utilizing silica optical fibers (SOFs), then polymer optical fibers (POFs). These devices did not need expensive optical apparatus and could be used to create a dense miniaturized device with remote sensing capabilities. Temperature [77], pressure [78,79], environmental monitoring [80,81], food safety [80,82], and biomedical applications [83–85], among others, all benefited from SPR-based optical sensing in recent years. An interesting review on plasmonic fiber optic biochemical sensors was recently published in [86], which addressed the recent developments in optical fiber-based, label-free recognition devices based on SPR effects.

For both labeled and label-free approaches, the use of optical-fiber devices as sensors provided several advantages such as size, cost, light path manipulation; nevertheless, those benefits were better reflected in label-free solutions because they offered total cost-saving and accessibility factors. Fiber-optic sensors, either as a hand-held probe or as a set of distantly controlled devices along a fiber-optic cable, might be placed into the media to be sensed, such as environmental monitoring applications [87]. In applications like pharmaceutical science, where many experiments must be conducted simultaneously, fiber-based diagnostics were not viable with bulk optic laboratory equipment like microplate array systems. Nevertheless, there appeared to be some promising applications where the fiber sensors' low cost and accessibility might guide to general adoption, for instance, testing for viral or bacterial diseases [88], testing for toxins in food handling plants, and examining the water quality in urban water supply structures or the atmosphere containing toxicogenic activities, and resource mining processes.

Various plasmonic sensors based on fiber-optics have lately been depicted based on the transmission probe, where noble metals were mounted on the etched cladding section, for instance, single-mode fibers (SMFs) [89], multi-mode fibers (MMFs) [90], wagon wheel fibers [91], U-shaped fibers [92,93], D-shaped fibers [94], and Bragg grating fibers [95], among others [96,97]. Biochemical reactions usually result in small RI changes in the ambient medium, and SPR-optic fiber devices are extremely vulnerable to these minor RI variations. As a result, these sensors became common in a variety of biosensing applications. An SPR-based optical fiber biomedical sensor for the recognition of CRP in serum was proposed [98,99]. Figure 8a illustrates a schematic of an SPR-optic fiber-based biosensors. When incident light passed through the fiber core with an incident angle larger than the critical angle, the evanescent field produced by the absolute reflection of the incident light revealed through the metal film at the same time. Strong light absorption happened as the parallel part of the incident light wave vector matched that of the SP wave. As a consequence, the output signal showed an SPR dip at a certain wavelength, defined as

the resonance wavelength. The photo of the fabricated SPR sensor is shown in Figure 8b. An SPR-optic fiber DNA biosensor was proposed in 2013 for the selection of DNA aptamers against the main peanut allergen protein, Ara h 1, which provided an alienation constant of 353 ± 82 nM [100]. In 2015, researchers demonstrated an extremely sensitive, label-free, and selective SPR-optic fiber-based glucose measuring device. It had a sensitivity of 1.514 nm $(mg/mL)^{-1}$ and could detect concentrations ranging from 0.1 to 2.5 mg/mL [101]. An SPR-optic fiber-based biochemical sensor for evaluating infliximab concentrations in the serum of inflammatory bowel illness patients was recently demonstrated, which provided a DL of 0.3 ng/mL [102].

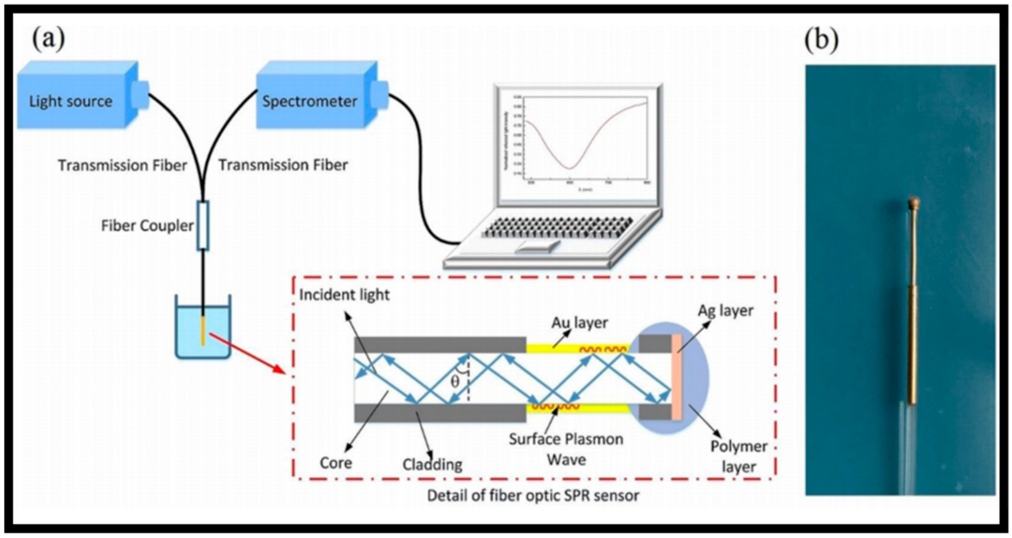

Figure 8. Surface plasmon resonance (SPR)-based fiber optic sensing technique: (**a**) graphic illustration of the experimental arrangement. Reprinted from ref. [99]; (**b**) picture of the manufactured fiber optic SPR sensor. Reprinted from ref. [99].

In 1978, the photonic crystal fiber (PCF) concept was proposed for the first time. It was proposed that a fiber core be clad with Bragg grating, which is like one-dimension (1D) [103]. The first PCF was reported in 1996 at the Optical Fiber Conference (OFC) [104], and it was composed of a 2D-PC with an air core. PCFs have a core and cladding that are identical to traditional optical fibers, but PCFs have a periodic air-hole in the cladding region that controls light propagation. Changing the geometry of air holes and the number of rings can be used to control the light propagation [105]. In [106], the first fiber-based plasmonic phenomenon was demonstrated by substituting graphene for the metal film and using thermal chemical vapor deposition (CVD) to produce a thin layer of graphene. An improvement in the sensing capability of SPR sensors with a graphene layer on top of Au/Ag was also demonstratable as compared to corresponding SPR sensors without the graphene layer [107–109]. The use of Au as an active plasmonic medium, as well as the selective penetration of the PCF core with a high RI to achieve the reconciliation of positive and negative index effects, was investigated [110]. D-shaped PCF sparked a lot of interest in SPR sensing due to its ease of production and utilization. The top surface of the fiber cladding was tailored to make it smooth, like how the metal layer and sample were mounted on top of the flat fragment in a D-shape. The metal layer in D-shape PCF could be placed close to the core, promoting close contact with the sample and improving system efficiency. Many D-shaped PCF sensors were developed to date for a variety of applications [111–115].

Sensing with PCF SPR is a promising and successful technology. These sensors, on the other hand, are still in the early stages of device production technology. Mainly, the findings in the studies used a proof-of-concept approach, as well as theoretical and computational models. Due to fabrication challenges, the usage of proven theoretical models for sensor

application was inadequate. Even though a few experimental procedures were published in the literature, their implementations are limited [116,117]. As a result, the empirical performances of the modeled sensors remain unexplored. Future research must concentrate on proving proof-of-concept for real PCF SPR sensor processing and analyte recognition for a wide variety of chemical and biological samples. One future advancement path for the PCF SPR sensors was transportable and instant lab-on-chip analyses for point-of-care diagnostics. The aim should be to switch existing fluorescence detecting with label-free PCF SPR detecting, enhancing the capability to detect a variety of analytes, reduce test expenditures, and conserve time by lowering sample formulation time. Unlike fluorescent sensors, the PCF SPR could be engineered to be redundant for purposes that need constant monitoring. As a result, PCF SPR device configurations should be made straightforwardly and cost-effectively.

A brief explanation concerning the metals employed in fiber SPR and LSPR technologies was discussed. Using well-recognized technologies like electroless deposition [118], electroplating [118], or sputtering [119], thin noble metal layers could be effectively placed on optical fibers. The last of these is most frequently used, and it delivers exceptionally high-quality metal thin films. A 5 nm to 10 nm chromium or titanium buffer layer is frequently inserted between the optical fiber surface and gold layer to enable adhesion. An alternative is to thermally anneal the gold coating, which adjusts its morphology and increases its durability [120]. It is crucial to remember that obtaining exceptionally uniform metal layers at the thickness needed for optimal SPR excitation (~50 nm) is difficult, and consequently, rugosity or fragments can form instead of smooth layers. Since the effective complex permittivity of the metal layers differed from that of the bulk values, this impacted the SPR properties (which were often used in the design of the sensors) [121]. The utilization of non-metal layers for plasmonic applications, for example, some forms of semiconductors and oxides, has been significant; current progress on the materials side, as discussed recently [122], still has to be investigated in fiber-based structures, although they exemplified promising research directions. An interesting review of alternative plasmonic materials beyond gold and silver was presented in [123].

Microstructured optical fibers (MOFs) are described by a sequence of air holes that run along the length of the fiber [124–126]. The geometry, size, and relative location of the air holes define the optical properties of this type of fiber. MOFs with high evanescent fields in the air holes can be built and manufactured by varying these parameters. The use of MOF in biochip applications was demonstrated for the first time in 2006 [127]. An optic-fluidic coupler chip made of PMMA polymer and fabricated with a CO_2 laser contained a 16 mm long fragment of MOF. The developed chip configuration allowed continuous liquid flow control and instantaneous optical characterization via the MOF. The MOF was functionalized to catch a particular single-stranded DNA string when inserted into the chip by immobilizing a sensing layer on the microstructured internal surfaces of the fiber. The sensing layer comprised a DNA string that was paired to the target DNA string, permitting extremely selective DNA hybridization. The evanescent wave sensing theory was used to detect the captured DNA optically. The presented method permitted the analysis of sample volumes as small as 300 nL and the production of miniaturized transportable devices due to the tiny chip size [127].

4. Metal-Insulator-Metal WG-Based Biosensors

Over the past few years, metal-insulator-metal (MIM) WG configuration has been widely studied due to its appropriateness for conducting SPP waves. SPPs are optical waves that travel along with a dielectric-metal boundary, making them interesting for several purposes [128–130]. SPPs are strictly constrained to dielectric-metal interfaces penetrating ~10 nm into metal (identified as skin depth) and usually more than 100 nm into dielectrics (depending on the wavelength). These WG structures can be combined with different shapes of air cavities to create a compact and dense RR configuration, which can be used in several applications [131–134], out of which biochemical sensing, for

example, the solution concentration and pH value, which can be evaluated through RI variations is the most widely studied topic. Compared to the other optical sensors, these structures have superior parameters of sensitivity and precision as well as much smaller dimensions. Several attempts were made to improve the size and shape of the resonator cavity, which could lead to better sensitivity and transmission, which in turn determined the quality factor (Q-factor) and figure of merit (FOM) of the sensor.

Recently, we presented several RI plasmonic sensor designs based on SPP waves to effectively use them in biomedical applications [17,37,135–142]. There were several other biomedical applications, such as photothermal therapy [143,144], blood group detection [145,146], glucose sensing [147,148], cancer cells [147], bacillus bacteria [147] that were also studied based on MIM WG configuration. Figure 9a–f shows unique sensor designs proposed by different researchers for RI sensing applications [17,140,149–152]. These sensors exhibit outstanding sensing performance, which incorporates high sensitivity (S), high-quality factor (Q-factor), and noteworthy figures of merit (FOM). The sensitivity (S) can be expressed as $S = \Delta\lambda/\Delta n$, where $\Delta\lambda$ is the change in λ_{res}, and Δn is the variance of the ambient RI. A noteworthy factor in a wavelength filter is the ability to have elevated wavelength selectivity, which signifies a high-quality factor (Q-factor). The Q-factor can be donated as $Q = \lambda_{res}/FWHM$, where FWHM is the full width at half-maximum of the transmittance spectrum. Likewise, FOM is determined as S/FWHM. A compact plasmonic coupled device based on a MIM WG has a single resonance cavity, as well as a clear and broadband tunable spectrum for sensing applications. As a result, optimizing the sensor configuration for the best performance is a critical problem in designing a plasmonic MIM WG RI sensor [153,154].

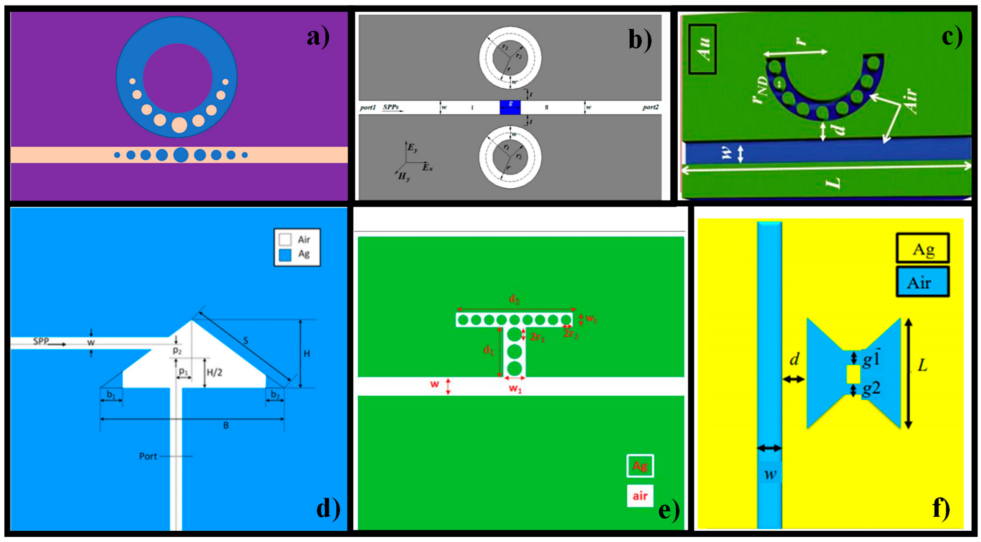

Figure 9. Recently proposed metal-insulator-metal (MIM) WG plasmonic sensors for biochemical applications: (**a**) RR coupled to a MIM WG containing tapered defects. Adapted from ref. [150]; (**b**) tunable plasmonic band-pass filter with dual side-coupled circular RRs. Reprinted from ref. [149]; (**c**) nanodots arranged MIM semi-RR cavity for biochemical sensing applications. Reprinted with permission from ref. [17]; (**d**) multiple Fano-like MIM plasmonic arrangement established on triangular resonator for refractive index (RI) sensing. Reprinted from ref. [151]; (**e**) MIM WG-coupled T-shape cavity with metal nanorod defects. Reprinted from ref. [152]; (**f**) plasmonic Bow-Tie configuration. Reprinted from ref. [140].

The expansion of analytical and numerical simulation software, for instance, COMSOL and Lumerical, which are commercially available, offered a better chance of understanding the optical characteristics of plasmonic sensor structures. Several systems, such as E-beam and ion beam lithography, could be used to fabricate nanostructures for plasmonic sensors, allowing for the lucrative fabrication of plasmonic devices over sizable regions.

Furthermore, wet chemical etching or vapor deposition methods might be used to simply manufacture metal nanoparticles. Nevertheless, the objective of this paper was not to go over these processes in-depth. As a substitute, we recommended a few review papers providing detailed knowledge on this important topic [155,156]. Two recent reports on the development of plasmonic sensors established on MIM WGs were provided [157,158] for the readers interested in obtaining detailed knowledge on their working mechanism, suitable materials, fabrication process, and applications.

5. Metasurfaces for Biosensing

Veselago anticipated the development of synthetic materials by manipulating their permittivity and permeability in 1968 [159]. This was finally discovered by the works of Pendry et al. [160] and Smith et al. [161], which made Veselago's hypothesis come true and revolutionized our perception of electromagnetics. These so-called metamaterials are artificial composite nanostructures with special characteristics for manipulating light and display a variety of stimulating novel optical effects and functions that natural materials cannot accomplish [162–165]. Metasurfaces (MSs) are structures that take advantage of the miniature footprint of metamaterials. They are fairly straightforward to produce and have a reduced size than traditional optical elements. They are made up of optical elements decorated on a surface with subwavelength sizes that form the wavefront of light to present an anticipated optical phase spatial profile which has directed to the invention of ultrathin optical elements with different capabilities that outperform their bulkier rivals [165,166]. Additionally, this new optical phenomenon demonstrates the EM spectrum spanning from visible to terahertz (THz) frequencies [167]. These MS-based flat systems constitute a new type of miniature, flat, and lightweight optical elements. Intensive research was conducted to employ MSs for biomedical applications [168–170].

All-dielectric asymmetric MSs, which are made up of groups of meta-atoms with broken in-plane inversion symmetry, have recently been discovered to have high-quality resonances resulting from the exciting physics of bound states in the continuum [171]. Dielectric MSs and hyperspectral imagining were merged in an intriguing approach to creating an ultrasensitive label-free analytical platform [169]. This method could collect high-throughput digital sensing data at an extraordinary level of fewer than 3 molecules/μm^2 by using smart data-processing tools and could collect the spatially solved spectra from millions of image pixels. This unique sensor architecture allowed spectral data extraction from a single image without the use of spectrometers, concreting the path for compact analytical applications. The potentials of dielectric MSs to analyze biological entities and atomic-layer thick 2D structures over wide areas were extended thanks to a fruitful amalgamation of nanophotonics and imaging optics. Spectral data recovery from a single image, devoid of applying spectrometers, supported by this exceptional sensor layout was demonstrated, paving the way for transportable diagnostic applications. Dielectric MSs could now analyze biological units and atom-layer thick 2D materials over wide areas thanks to a fusion of nanophotonics and imaging optics. A new category of RI sensor established on all-dielectric gradient MS was proposed and analyzed. A unique approach of optical data processing, which was established on intensity distribution over several diffraction orders, was proposed. The intensity of 4450%/RIU and the phase sensitivity of 1200º/RIU were demonstrated [172]. The sensor design based on gradient MS is demonstrated in Figure 10a,b [172].

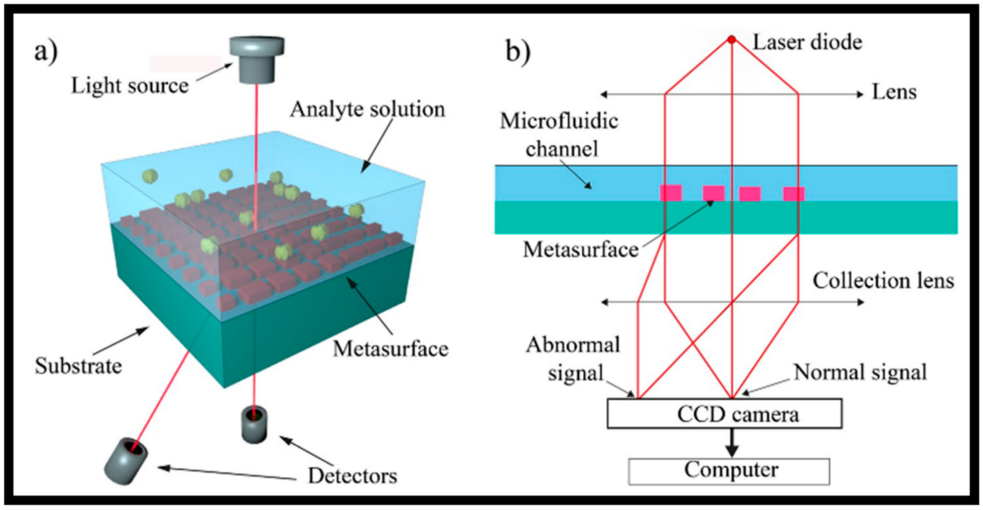

Figure 10. (**a**) The design of sensor-based on gradient metasurface (MS). Reprinted with permission from ref. [172]; (**b**) possible optical sensing scheme. Reprinted with permission from ref. [172].

Endoscopic optical imaging with high resolution is a well-known technique in biological imaging for analyzing inner organs. Optical coherence tomography (OCT) is an imaging procedure that can acquire tissue microstructures at millimeter depths in the tissues and has been employed for clinical diagnosis in head and neck cancer, cardiovascular disorders, and dermatology. OCT detects changes in the sample's RI using a low-coherence light interferometry setup and, thus, provides morphological details. A medical endoscopic optical imaging system established on OCT with a metalens was developed [173]. It discussed the problems of spherical and chromatic aberration, all of which were unacceptable. There were some other notable works on MSs based flat optics [174–176] and endoscopic optical imaging [177,178]. MS biosensors were also used to identify cancer biomarkers, such as breast, liver, and oral cancer. For the recognition of breast cancer biomarkers, an optofluidic MS biosensor was created [179]. Another example was the assessment of biomarkers for liver cancer [180]. The apoptosis of oral cancer cells was analyzed using an electromagnetically induced transparency (EIT) like MS [181].

Wearable sensor technology is a critical connection to personalized medicine in the future. It is important to acquire a full picture of human health; however, tracking several analytes within the body at the same time is difficult. The researchers depicted a wearable plasmonic-electronic sensor with universal molecular identification capability [182]. Since the practical task of preserving the plasmonic activities of the fragile nanostructures under different distortions was resolved, a compliant plasmonic MS with SERS-activity was established as the basic sensing module in a wearable device. The proposed sensor, when used in conjunction with a versatile electronic sweat removal system, could non-invasively extract and fingerprint analytes within the body established on their spectral SERS spectra. The variety of trace-amount drugs within the body was effectively tracked, and an individual's drug metabolic profile was obtained as a proof-of-concept illustration. By offering a universal, responsive molecular examining means to evaluate human health, the sensor filled a void in wearable sensing technology [182]. An attractive design of a wearable electronic nose for armpit odor testing was suggested in [183] by utilizing an economical chemical sensor array incorporated in a ZigBee wireless communication network. Figure 11a describes the model of the fabricated wearable e-nose. The mask kept the sensor surface from rubbing but permitted the free passage of the air and odors. The body odor could be easily gathered from the armpit area using this sensor. The sensor resistance as a function of the displayed VOCs and their concentrations were used to verify the odor data. The system used ZigBee technology to transmit data from the sensor to the computer, which is well known as a low-cost wireless network communication [183]. In [184], a wearable and adaptable pressure sensor design was proposed, which was critical

for the continuous monitoring of a person's health. It showed an excellent performance with the accord of numerous qualities, containing high sensitivity for a broad pressure range and an ultralow energy intake level of 10^{-6} W. Furthermore, pressure sensors might be incorporated onto robots as artificial skins, allowing them to feel pressure and the dispersal of pressure through the synthetic skin. The sensor was attached to the artery vessel at the wrist, as shown in Figure 11b, to reveal their potential of detecting human vital physiological signals [184]. The optical images of the assembled unit are revealed in Figure 11c,d, and the pressure provided excellent versatility. After being decorated with single-walled nanotubes, the sheet resistance of paper sheets decreased to about12.6 kΩ, which was adequately conductive to be used as an active layer in a pressure sensor [184].

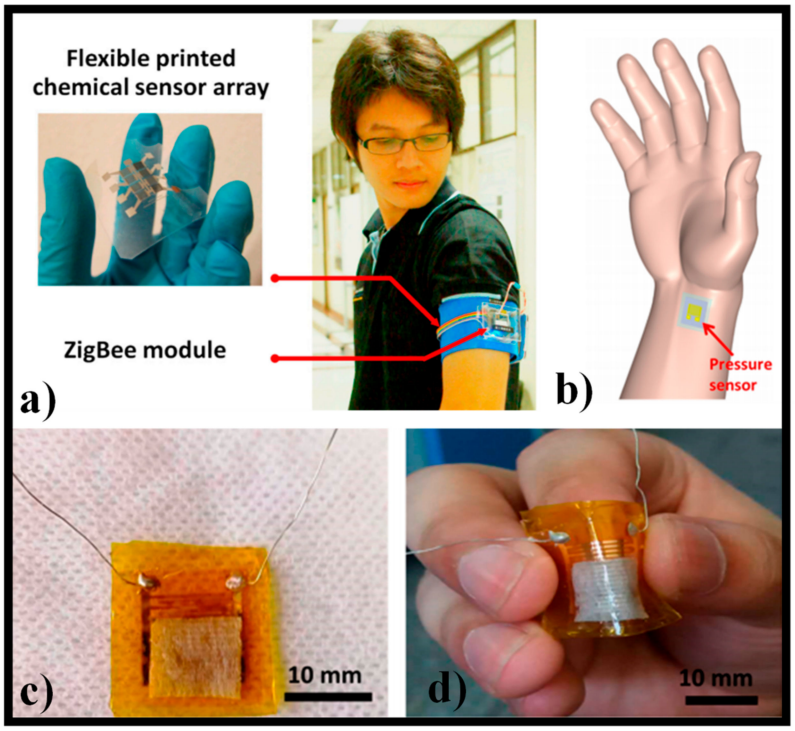

Figure 11. **(a)** Model of a wearable e-nose established on the adaptable inkjet-printed chemical sensor array incorporated in ZigBee wireless network. Reprinted from ref. [183]; (**b**) pressure sensor was attached to a human wrist for heart pulse detection. Reprinted from ref. [184]; (**c**) photograph of a manufactured pressure sensing device connected with Al wires. Reprinted from ref. [184]; (**d**) photograph of a bent pressure sensing device. Reprinted from ref. [184].

6. Photonic Crystals-Based Biosensors

Biomarkers have been detected using sensitive biosensing technologies such as SPR, electrochemical biosensors, and, more newly, inverse opal photonic crystal (PhCs) biosensors [185–187]. The invention of PhCs in 1987 by Yablonovitch [188] and John [189] sparked a lot of interest. EM waves propagated inside the PhC, and disruptive interference occurred for certain wavelengths, resulting in a photonic bandgap (PBG), which was close to the energy bandgap of electron waves in a semiconductor. It might be possible to control light propagation due to the likelihood of producing PBG. Light bending [190–192], optical diode [193], negative refraction [194], and self-collimation [195] were only a few of the notable applications of PhCs. Currently, PhCs biosensors were employed to identify a wide range of biological analytes selectively and sensitively, including DNA, cells, bacteria, proteins, and antibodies. This allowed for improved sensing efficiency concerning limit-of-detection (LOD) [196].

Various studies in PhC bioassays and their usage in bio-systems have been published to date, with an emphasis on the physical and optical activity of PhCs [197,198]. In [199],

a detailed description and understandings of the inverse opal bio-sensing procedures for detecting biological factors such as viruses, proteins, and DNA were presented. Photonic Bragg diffraction planes could be formed in inverse opal structures with periodic arrays because of high and low dielectric zones. The photonic band's optical properties contributed to their use in bio-sensing systems. By binding biomarkers to pore surfaces or flowing liquids through inverse opal pores, the detection process in inverse opal configurations was associated with a shift in RI in the pores and voids of inverse opal films. These variations preceded the blue/red shift in PBG in reflected wavelength spectra and color modifications in inverse opal thin-films [200]. The porous structure of the inverse opal created a large surface area for small molecule recognition. The optical properties of the exceedingly ordered inverse opal were supposed to be fine. Optical investigations revealed that different pore sizes in inverse opal resulted in different reflection or transmission spectra [201,202].

Due to their potency in portable point-of-care-testing tools and color metrics for graphical biosensor applications, inverse opal label-free materials are appealing and appropriate sensing systems for the recognition of proteins. Inverse opals may be used to diagnose biological particles without the use of advanced research tools because of their intuitive structural color [203]. The detection of alpha-fetoprotein (AFP), a liver cancer biomarker, was proposed using a photoelectrochemical biosensor founded on ZnO inverse opal with a LOD of 0.01 ng/mL. ZnO inverse opal and quantum dots were used on the photoelectrochemical electrode surface in this analysis [204]. In another study, an inverse opal biosensor based on inverse opal-Ag_2S NPs was proposed for the detection of AFP [205]. The ZnO inverse opal/Ag_2S composite resulted in the production of long-wavelength light absorption. The LOD for AFP detection was 8 pg/mL, which was nearly 1.5 times higher than the former process. This outcome was due to better photo-generated electron conduction in ZnO inverse opal/Ag_2S structures due to the successful matching of energy levels among the transmission bands of Ag_2S and ZnO inverse opal [205]. Apart from the TiO_2 based inverse opal, IOH nonporous arrangements could be employed in label-free and selective recognition of the IgG antibodies [206]. With increasing IgG concentration, the color of the IOH structure shifted from green to orange, which could be seen with the naked eye, as well as a 50 nm bandgap shift in absorbance spectra.

Utilizing self-assembled Au nanoparticles conjugated with biotinylated anti-gp120 polyclonal antibodies to particularly capture and identify HIV, a nanoplasmonic-based platform was designed [207]. Via impedance spectroscopy of viral lysate samples, an electrical sensing process was established to identify captured HIV-1 on magnetic beads coupled with anti-gp120 antibodies [208]. PhC biosensors, for example, use dielectric permittivity variations at the interface of a transducer substrate and a liquid media to provide a fast and precise optical recognition procedure for biomolecules, cells, and viruses [209]. In this case, optical detection using PhC biosensors for instantaneous monitoring of virus infection can be more valuable than laborious pathogen-specific molecular recognition methods such as polymerase chain reaction (PCR) and enzyme-linked immunosorbent assay (ELISA). The unharmed virus particles in actual test samples were detected using instant and responsive viral PhC sensing procedures that did not involve labeling or multiple chemical alteration methods. By immobilizing antibodies on the periodic arrangements of the PhC surface, a reflectometric 2D PhC biosensor was developed for the recognition of the influenza virus in human saliva with a LOD of 1 ng/mL [210].

Early discovery of the virus applying non-invasive, high-sensitivity, and innovative bio-sensing methods was highly successful in keeping the individual safe from viral infections [211]. As shown in Figure 12a, the periodic composition of dielectric material on a PhC sensor caused the formation of an optical resonance at a specific wavelength, at which EM standing waves spread into the liquid media in contact with the PhC surface. The PhC nanostructures were created by replica molding of a low index polymer, which was then covered with a high index TiO_2 dielectric layer to form a periodic surface structure. When lit up with a paralleled broadband light at a normal incidence angle, the PhC configuration reflected only a small resonant band of light with practically 100% efficacy, whereas all

other wavelengths were transmitted. When biological samples like proteins, viruses, or cells connected to the PhC, the peak wavelength value (PWV) of the reflected resonant continuum moved to a greater value, as shown in Figure 12b.

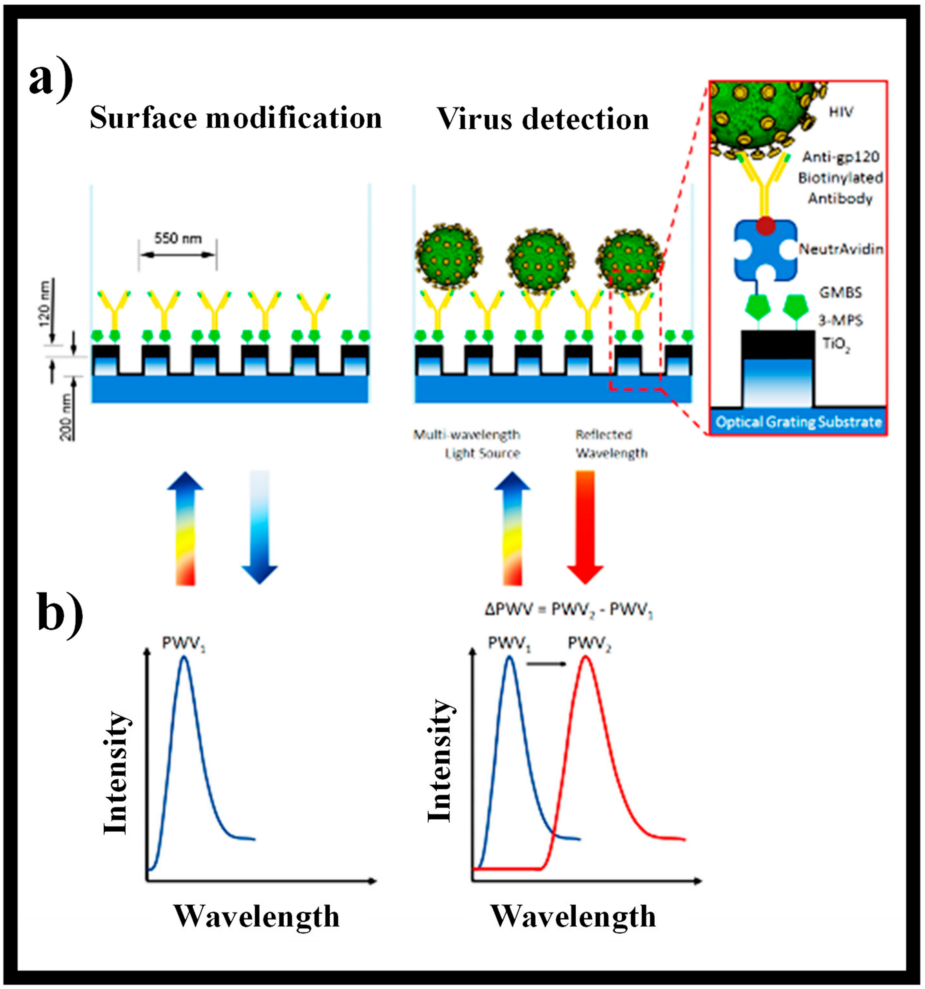

Figure 12. Schematic of PhC-based virus recognition platform. (**a**) The bottom surface of PhC biosensor microplate wells is made up of a nanostructured subwavelength grating that is covered with TiO_2. Reprinted from ref. [211]; (**b**) binding occurrences inside the immediate proximity of the sensing area alter the bulk RI; therefore, the peak wavelength value (PWV) of the reflected light is changed. The swing in the peak wavelength (DPWV) is in direct proportion to the attachment of molecules and/or bioagents onto the biosensing surface Reprinted from ref. [211].

7. Photonic Biosensing with Thin Metal Films

Sample handling, biological detection and amplification, transduction, and electronic signal processing are all areas where thin films are used in biosensor systems [212,213]. Several planar microelectrochemical chips on Si or glass substrates with thin-film electrodes of various shapes and arrangements have been developed and utilized in voltammetric and potentiometric sensors. Bilayer lipid membranes (BLMs) are thin-film materials that are flexible and can be used in biosensors [214,215]. The use of thin-film electrodes to develop BLMs on a planar chip revealed new possibilities to produce miniaturized biosensors along with basic research into the electrical and mechanical properties of biological membranes. It was 30 years ago that the first effort to build BLMs was made [216]. However, the solvent was held in the structure of the membranes, and the results cannot be replicated. Methods for making solvent-free lipid membranes were also presented, but their main downside was that these films were extremely brittle and susceptible to collapse when

subjected to mechanical or electrical shock [217]. The literature documented methods to enhance the constancy of these lipid films, such as interconnected membrane bubbles in organic solvents without a substrate aperture or the so-called monolayer technique [218].

Biosensors of the current generation are analytical lightweight instruments made of thin films. The main benefits of these biosensors are their sensitivity, accuracy, rapid response time, accessibility, and small cost. All these characteristics are closely linked to the thickness of the films used in the sensor fabrication [219]. The interaction of the biological analyte with the surface-modified thin film is the key basis for a biosensor's detection principle. The thin film functions as a physiochemical-optical, mechanical, magnetic, and electrical transducer, converting the signal produced by the biological analyte recognition into another observable signal [220]. SPR spectroscopy is a well-known analytical method for quantifying molecular interactions at an interface without using labels. The technique works by identifying slight variations in RI of a dielectric medium in contact with a thin metal film on the nanometer scale. Gold (Au) has historically been used as the metal layer because of its elevated plasmonic activity and chemical inertness. Further, metals such as chromium (Cr), copper (Cu), and aluminum (Al), on the other hand, are receiving more attention as plasmonic materials. Al has a higher electron density and a higher negative permittivity than Ag or Au, making it remarkably interesting [221]. Al is plasmonically active from the UV to the near IR regions due to this attribute, which causes plasmonic resonance over a broad wavelength range [222]. Al is also attractive for industrial applications because of its abundant supply, low cost, and ease of incorporation into manufacturing processes like CMOS.

In [223], SPR biosensing with Al thin-films was demonstrated employing the traditional Kretschmann structure that had formerly been overshadowed by Au films [224]. In both bulk and surface samples, Al films displayed excellent sensitivity efficiency in both classifications. In comparison to Au, the Al/Al_2O_3 layer had a significant effect on controlling nonspecific binding in blood serum. When used for SPR imaging research, Al film had a higher sensitivity and a broader working range than Au films, according to further characterization. The Al thin-film, when combined with its cost and processing advantages, can become an extremely beneficial plasmonic substrate for a large range of biosensing functions in SPR formations. In [225], the cholesterol sensors comprising of a blend of cholesterol oxidase (ChOx) and zinc oxide (ZnO) nanoparticles were cultivated on ITO/glass substrates by thermal evaporation technique, and their sensing attributes are analyzed in air.

In [226], an ellipsometry study on gold nanoparticles (AuNPs) coated on Au thin film was demonstrated for biosensing applications. The SPR dip could be tuned from the visible to near-IR merely altering the AuNP concentration. Figure 13a reveals the SEM photograph of the distribution of the AuNPs on the gold surface after a 1-min treatment of the amine-functionalized gold substrate. These samples were placed on the dove prism using a microfluidic flow cell to comprehend the optical properties of different AuNPs' distribution immobilized on the Au substrate in water. Figure 13b depicts the architecture of the experimental setup in the TIR arrangement. With this system, the optical response of various samples was measured using ellipsometry signals (Ψ, Δ). Bulk sensitivity tests were performed to calibrate the SPR unit based on ellipsometric signals (Ψ and Δ) and by infusing glycerol-water mixtures of different concentrations with different RI values onto the sensing surface via the microfluidic flow cell as indicated in Figure 13c,d. A refractometer was utilized to measure the RI values of various glycerol-water mixtures.

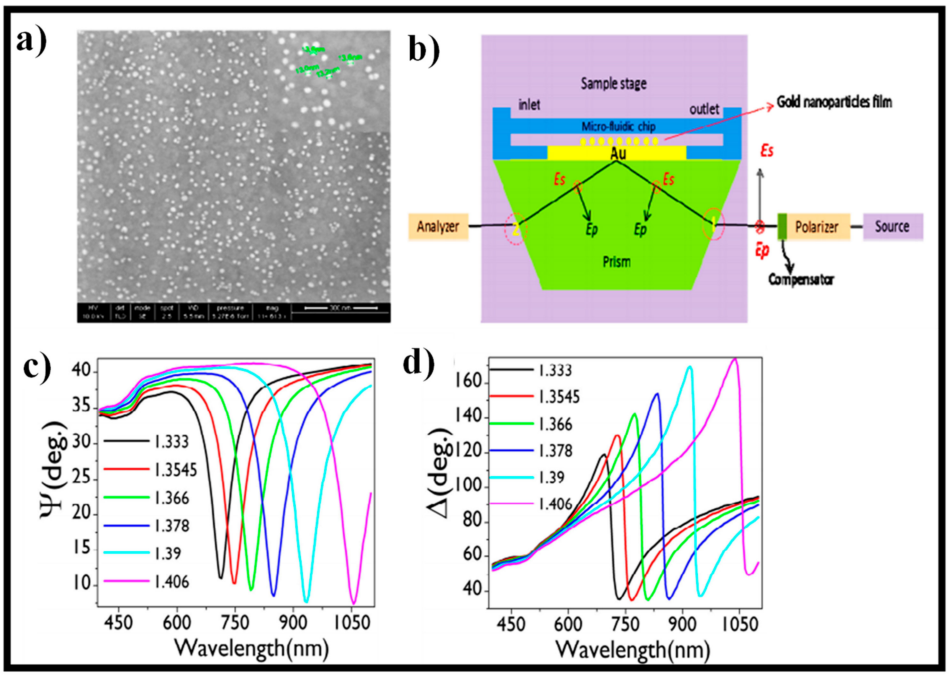

Figure 13. (**a**) Distribution of AuNPs on the Au surface after 1-min treatment of amine-functionalized Au substrate. Reprinted from ref. [226]; (**b**) graphical illustration of the experimental setup with optical components showing the polarization of the incident and reflected light within the prism for a sample attached perpendicular to the sample stage. Reprinted from ref. [226]; (**c**,**d**) spectral response of the ellipsometric parameters Ψ, Δ for glycerol-water mixtures having different refractive indices introduced on 30 min treated AuNPs-coated Au substrate. Reprinted from ref. [226].

8. Fiber Bragg Grating Biosensors

Researchers have so far investigated fiber grating sensors, some of which are now commercially available. Fiber Bragg grating (FBG), long-period grating (LPG), chirped fiber grating (CFG), tilted fiber Bragg grating (TFBG), etched fiber Bragg grating (EFBG), and sampled fiber grating (SFG) are the different kinds of fiber gratings, with FBG being the most common in sensor design [227,228]. FBGs may be photo imprinted onto fibers, and the resulting FBG sensors are usually strain and temperature-sensitive. High sensitivity, multiplexing capability, compact size, multi-modal sensing ability, tolerance to EM intervention, and low production cost are all advantages of optical fiber grating-based sensors. Owing to their label-free design of quantifying RI, optical grating sensors such as LPG, EFBG, and TFBG sensors are becoming more common in the development of chemo- and biosensors [229]. Some of these FBG biosensor configurations have been tested in the hopes of improving thrombin biosensors [230,231]. Thrombin is involved in both normal and abnormal coagulation, and its normal concentration ranges from nanomolar to low micromolar during blood coagulation [232]. Thrombin levels can rise when tumor cells cause blood coagulation both extra- and intravascularly. Thrombin is implicated in a variety of diseases, including atherosclerosis, thromboembolic disease, cancer, and inflammatory disease, so finding it in the blood is crucial for both study and clinical applications [233]. Because of its clinical significance, there has been a lot of research into detecting thrombin, with the bulk of it focusing on aptamers.

An FBG sensor, on the other hand, cannot conduct RI-based sensing because the optical field is limited to the fiber core [234]. For this purpose, the evanescent field must interact with the ambient medium, which can be accomplished by polishing [85], etching [235], or tapering the fiber [236]. The wavelength response of the Bragg grating, which is determined by the bulk RI, will appear when the FBG is immersed in a sample liquid. In [237], hydrofluoric acid (HF) was used to etch the fiber cladding at the Bragg grating points, which amplified the light-matter interaction. For RI bulk sensing, a thinned FBG

sensor was presented [238]. The experiment used glycerin solutions with well-recognized RIs to assess sensor sensitivity. A highly sensitive etched-core FBG sensor was proposed, which detected any external RI change by measuring the shift in λ_{Bragg}. The sensitivity value was 1394 nm/RIU when the fiber core was reduced to a diameter of 3.4 µm, and the RI of the surrounding area was like that of the fiber core [239]. Higher-order modes yielded higher sensitivity in detection when the RI of the surrounding was less than that of the fiber core, e.g., the second-order mode yielded a sensitivity of 404 nm/RIU compared to the fundamental mode's sensitivity of 171 nm/RIU. Finally, the FBG sensor was used to detect DNA molecule hybridization. The hybridization of target DNA molecules was observed, and a wavelength shift of 73 pm, equivalent to a RI change of 2.5×10^{-3}, was measured. The in-situ monitoring of bioprocesses was possible with this FBG sensor [239].

FBG biosensors can be employed as a cost-effective and comparatively simple-to-realize option to well-established biosensor platforms for superior sensitivity biological sample measurements in situ or probably in vivo [240]. A fiber biosensor employs an in-fiber 12° tilted Bragg grating to stimulate a robust evanescent field on the sensor's surface over a wide range of outer medium RIs. Human acute leukemia cells with different intercellular densities and RIs ranging from 1.3342–1.3344 were unambiguously distinguished in situ by utilizing the differential transmission continuum between orthogonal polarizations. An amplitude deviation sensitivity, wavelength variation sensitivity and LOD were 1.8×10^4 dB/RIU, 180 nm/RIU, and LOD of 2×10^{-5} RIU were obtained, respectively. A microfluidic chip that allows the measurement of nL-volumes of biosamples was used to precisely monitor the detection process, as shown in Figure 14a [240]. The proposed in-fiber polarimetric biosensor was an appealing solution for rapid, sub-µL dose highly sensitive detection of analytes at low concentrations in medicine, chemical, and environmental monitoring. Figure 14b shows a graphical representation of a TFBG biosensor probed with tunable linearly polarized light [240].

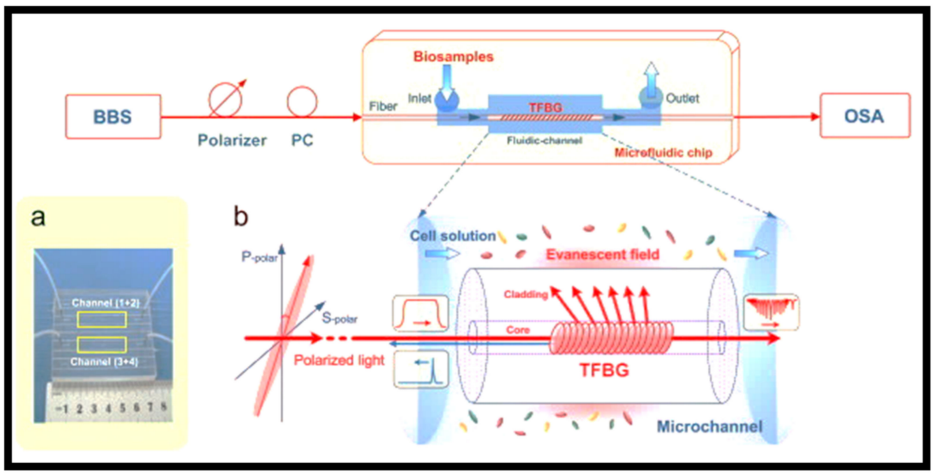

Figure 14. Polarimetric tilted fiber Bragg grating (TFBG) sensing system: (**a**) micro-fluidic chip for biosample measurements. Reprinted with permission from ref. [240]; (**b**) schematic diagram of polarimetric TFBG biosensor interrogated with tunable linearly polarized light. Reprinted with permission from ref. [240].

9. Conclusions

The optical biomedical sensor industry has grown enormously over the past few years and is expected to grow more in the forthcoming days because of the extensive need for point-of-care testing devices. Researchers all over the world are working on the implementation of highly sensitive, reliable, portable, and inexpensive biomedical appliances, which can revolutionize this market. Optical biosensing is a vast topic, and numerous optical sensing techniques have been presented over the years. It is difficult to enclose all of these methods in one place. That's why we selected a few prominent optical biomedical

sensing methods which potentially could interest our readers. Herein, a brief review of optical sensors was presented such as Mach–Zehnder interferometer, Young's interferometer, ring resonators, vertical grating couplers, surface plasmon resonance optical fiber biosensors, metasurfaces biosensors, metal-insulator-metal waveguide-based biosensors, photonic crystal biosensor, plasmonic biosensing with metal thin films, and fiber Bragg grating biosensors. Our main goal was to enlist the merits and demerits of each sensing method without offering any final verdict in favor of any particular sensing method.

Author Contributions: Conceptualization, N.L.K., S.N.K., M.A.B.; methodology, N.L.K., S.N.K., M.A.B.; software, N.L.K., S.N.K., M.A.B.; validation, N.L.K., S.N.K., M.A.B.; formal analysis, M.A.B.; investigation, M.A.B.; resources, M.A.B., A.K., R.P.; data curation, M.A.B.; writing—original draft preparation, M.A.B.; writing—review and editing, N.L.K., S.N.K., M.A.B., A.K., R.P.; visualization, N.L.K., S.N.K., M.A.B., A.K., R.P.; supervision, N.L.K., S.N.K., M.A.B.; project administration, N.L.K., S.N.K., M.A.B.; funding acquisition, N.L.K. All authors have read and agreed to the published version of the manuscript.

Funding: This work was financially supported by the Ministry of Science and Higher Education of the Russian Federation (the scientific state assignment No. 0777-2020-0017 of the Samara National Research University) for numerical calculations, by the FSRC 'Crystallography and Photonics´ of the Russian Academy of Sciences (the state task No. 007-GZ/Ch3363/26) for theoretical research, and by the Russian Science Foundation (grant No. 20-69-47110) for comparative analysis. Additionally, this work was done within the framework of 'Hybrid sensor platforms of integrated photonic systems based on ceramic and polymer materials´ project is carried out within the TEAM-NET program of the Foundation for Polish Science financed by the European Union under the European Regional Development Fund, POIR.04.04.00-00-14D6/18-01.

Acknowledgments: We acknowledge the equal support from all the authors.

Conflicts of Interest: The authors declare no conflict of interest.

References

1. Available online: globenewswire.com (accessed on 15 March 2021).
2. Yu, D.; Blankert, B.; Vire, J.; Kauffmann, J.; Blankert, J.P. Biosensors in Drug Discovery and Drug Analysis. *Anal. Lett.* **2005**, *38*, 1687–1701. [CrossRef]
3. Thakur, M.S.; Ragavan, K.V. Biosensors in food processing. *J. Food Sci. Technol.* **2013**, *50*, 625–641. [CrossRef] [PubMed]
4. Gil, E.D.; Melo, G.R. Electrochemical biosensors in pharmaceutical analysis. *Braz. J. Pharm. Sci.* **2010**, *46*, 375–391. [CrossRef]
5. Sadana, A.; Sadana, N. Market size and economics for biosensors. In *Fractal Analysis of the Binding and Dissociation Kinetics for Different Analytes on Biosensor Surfaces*; Elsevier: Amsterdam, The Netherlands, 2008; pp. 317–334.
6. Clark, L. Monitor and control of blood and tissue oxygen tensions. *Trans. Am. Soc. Artif. Internal Organs* **1956**, *2*, 41–46.
7. Chun, H.J.; Han, Y.D.; Park, Y.M.; Kim, K.R.; Lee, S.J.; Yoon, H.C. An optical biosensing strategy based on selective light absorption and wavelength filtering from chromogenic reaction. *Materials* **2018**, *11*, 388. [CrossRef] [PubMed]
8. Ligler, F.S. Fluorescence-based optical biosensors. In *Biophotonics*; Springer: Berlin/Heidelberg, Germany, 2008; pp. 199–215.
9. Chen, Y.; Liu, J.; Yang, Z.; Wilkinson, J.S.; Zhou, X. Optical biosensors based on refractometric sensing schemes: A review. *Biosens. Bioelectron.* **2019**, *144*, 111693. [CrossRef] [PubMed]
10. Maisonneuve, M.; Song, I.-H.; Patskovsky, S.; Meunier, M. Polarimetric total internal reflection biosensing. *Opt. Express* **2011**, *19*, 7410–7416. [CrossRef]
11. Hutchinson, A.M. Evanescent wave biosensors. *Mol. Biotechnol.* **1995**, *3*, 47–54. [CrossRef]
12. Taitt, C.R.; Anderson, G.P.; Ligler, F.S. Evanescent wave fluorescence biosensors: Advances of the last decade. *Biosens. Bioelectron.* **2016**, *76*, 103–112. [CrossRef]
13. Huertas, C.S.; Calvo-Lozano, O.; Mitchell, A.; Lechuga, L.M. Advanced evanescent-wave optical biosensors for the detection of nucleic acids: An analytic perspective. *Front. Chem.* **2019**, *7*, 724. [CrossRef]
14. Zhang, Z.; Li, Q.; Du, X.; Liu, M. Application of electrochemical biosensors in tumor cell detection. *Thorac. Cancer* **2020**, *11*, 840–850. [CrossRef] [PubMed]
15. Villiger, M.; Stoop, R.; Vetsch, T.; Hohenauer, E.; Pini, M.; Clarys, P.; Pereira, F.; Clijsen, R. Evaluation and review of body fluids saliva, sweat and tear compared to biochemical hydration assessment markers within blood and urine. *Eur. J. Clin. Nutr.* **2017**, *72*, 69–76. [CrossRef] [PubMed]
16. Lee, S.H.; Cho, Y.C.; Choy, Y.B. Noninvasive self-diagnostic device for tear collection and glucose measurement. *Sci. Rep.* **2019**, *9*, 4747. [CrossRef]
17. Kazanskiy, N.; Butt, M.; Khonina, S. Nanodots decorated MIM semi-ring resonator cavity for biochemical sensing applications. *Photon. Nanostructures Fundam. Appl.* **2020**, *42*, 100836. [CrossRef]

18. Butt, M.A.; Kazanskiy, N.L.; Khonina, S.N. Label-free detection of ambient refractive index based on plasmonic Bragg gratings embedded resonator cavity sensor. *J. Mod. Opt.* **2019**, *66*, 1920–1925. [CrossRef]
19. Xie, Y.; Zhang, M.; Dai, D. Design Rule of Mach-Zehnder Interferometer Sensors for Ultra-High Sensitivity. *Sensors* **2020**, *20*, 2640. [CrossRef]
20. Kalbarczyk, A.; Jaroszewicz, L.R.; Bennis, N.; Chrusciel, M.; Marc, P. The Young Interferometer as an Optical System for a Variable Depolarizer Characterization. *Sensors* **2019**, *19*, 3037. [CrossRef]
21. Yi, H.; Citrin, D.S.; Chen, Y.; Zhou, Z. Dual-microring-resonator interference sensor. *Appl. Phys. Lett.* **2009**, *95*, 191112. [CrossRef]
22. Butt, M.A.; Khonina, S.N.; Kazanskiy, N.L. Device performance of standard strip, slot and hybrid plasmonic μ-ring resonator: A comparative study. *Waves Random Complex Media* **2020**, 1–10. [CrossRef]
23. Heideman, R.; Kooyman, R.; Greve, J. Development of an optical waveguide interferometric immunosensor. *Sens. Actuators B Chem.* **1991**, *4*, 297–299. [CrossRef]
24. Liu, Q.; Tu, X.; Kim, K.W.; Kee, J.S.; Shin, Y.; Han, K.; Yoon, Y.-J.; Lo, G.-Q.; Park, M.K. Highly sensitive Mach–Zehnder interferometer biosensor based on silicon nitride slot waveguide. *Sens. Actuators B Chem.* **2013**, *188*, 681–688. [CrossRef]
25. Mahmudin, D.; Huda, N.; Estu, T.T.; A Fathnan, A.; Daud, P.; Hardiati, S.; Hasanah, L.; Wijayanto, Y.N. Design of optical channel waveguide Mach-Zehnder interferometer (MZI) for environmental sensor applications. *J. Phys. Conf. Ser.* **2017**, *817*, 12036. [CrossRef]
26. Lee, J.-M. Ultrahigh Temperature-Sensitive Silicon MZI with Titania Cladding. *Front. Mater.* **2015**, *2*, 36. [CrossRef]
27. Lin, B.; Yi, Y.; Cao, Y.; Lv, J.; Yang, Y.; Wang, F.; Sun, X.; Zhang, D.; Lin, Y. A Polymer Asymmetric Mach–Zehnder Interferometer Sensor Model Based on Electrode Thermal Writing Waveguide Technology. *Micromachines* **2019**, *10*, 628. [CrossRef] [PubMed]
28. Brandenburg, A.; Henninger, R. Integrated optical Young interferometer. *Appl. Opt.* **1994**, *33*, 5941–5947. [CrossRef] [PubMed]
29. Brandenburg, A.; Krauter, R.; Künzel, C.; Stefan, M.; Schulte, H. Interferometric sensor for detection of surface-bound bioreactions. *Appl. Opt.* **2000**, *39*, 6396–6405. [CrossRef] [PubMed]
30. Schmitt, K.; Schirmer, B.; Hoffmann, C.; Brandenburg, A.; Meyrueis, P. Interferometric biosensor based on planar optical waveguide sensor chips for label-free detection of surface bound bioreactions. *Biosens. Bioelectron.* **2007**, *22*, 2591–2597. [CrossRef]
31. Uusitalo, S.; Känsäkoski, M.; Karkkainen, A.H.O.; Hannu-Kuure, M.; Aikio, S.; Kopola, H. Biosensing with Low-Index Waveguides: An Experimental Study of a Polymer-Based Young Interferometer Sensor. *Micro Nanosyst.* **2010**, *2*, 65–69. [CrossRef]
32. Hiltunen, M.; Hiltunen, J.; Stenberg, P.; Aikio, S.; Kurki, L.; Vahimaa, P.; Karioja, P. Polymeric slot waveguide interferometer for sensor applications. *Opt. Express* **2014**, *22*, 7229–7237. [CrossRef]
33. Luan, E.; Shoman, H.; Ratner, D.M.; Cheung, K.C.; Chrostowski, L. Silicon Photonic Biosensors Using Label-Free Detection. *Sensors* **2018**, *18*, 3519. [CrossRef]
34. Janeiro, R.; Flores, R.; Viegas, J. Silicon photonics waveguide array sensor for selective detection of VOCs at room temperature. *Sci. Rep.* **2019**, *9*, 17099. [CrossRef] [PubMed]
35. Zinoviev, K.; Carrascosa, L.G.; Del Río, J.S.; Sepúlveda, B.; Domínguez, C.; Lechuga, L.M. Silicon Photonic Biosensors for Lab-on-a-Chip Applications. *Adv. Opt. Technol.* **2008**, *2008*, 1–6. [CrossRef]
36. Butt, M.A.; Khonina, S.N.; Kazanskiy, N.L. Hybrid plasmonic waveguide-assisted Metal–Insulator–Metal ring resonator for refractive index sensing. *J. Mod. Opt.* **2018**, *65*, 1135–1140. [CrossRef]
37. Butt, M.A.; Khonina, S.N.; Kazanskiy, N.L. Highly sensitive refractive index sensor based on hybrid plasmonic waveguide microring resonator. *Waves Random Complex Media* **2018**, *30*, 292–299. [CrossRef]
38. Sun, Y.; Fan, X. Optical ring resonators for biochemical and chemical sensing. *Anal. Bioanal. Chem.* **2010**, *399*, 205–211. [CrossRef] [PubMed]
39. Su, J. Label-Free Biological and Chemical Sensing Using Whispering Gallery Mode Optical Resonators: Past, Present, and Future. *Sensors* **2017**, *17*, 540. [CrossRef] [PubMed]
40. Kazanskiy, N.; Butt, M.; Khonina, S. Silicon photonic devices realized on refractive index engineered subwavelength grating waveguides-A review. *Opt. Laser Technol.* **2021**, *138*, 106863. [CrossRef]
41. Butt, M.A.; Khonina, S.N.; Kazanskiy, N.L. Ultrashort inverted tapered silicon ridge-to-slot waveguide coupler at 155 μm and 3392 μm wavelength. *Appl. Opt.* **2020**, *59*, 7821–7828. [CrossRef]
42. Carlborg, C.F.; Gylfason, K.; Kazmierczak, A.; Dortu, F.; Polo, M.J.B.; Catala, A.M.; Kresbach, G.M.; Sohlström, H.; Moh, T.; Vivien, L.; et al. A packaged optical slot-waveguide ring resonator sensor array for multiplex label-free assays in labs-on-chips. *Lab Chip* **2010**, *10*, 281–290. [CrossRef]
43. A Butt, M.; Khonina, S.N.; Kazanskiy, N.L. A highly sensitive design of subwavelength grating double-slot waveguide microring resonator. *Laser Phys. Lett.* **2020**, *17*, 076201. [CrossRef]
44. Kazanskiy, N.L.; Khonina, S.N.; Butt, M.A. Subwavelength Grating Double Slot Waveguide Racetrack Ring Resonator for Refractive Index Sensing Application. *Sensors* **2020**, *20*, 3416. [CrossRef]
45. Badri, S.H. Transmission resonances in silicon subwavelength grating slot waveguide with functional host material for sensing applications. *Opt. Laser Technol.* **2021**, *136*, 106776. [CrossRef]
46. Flueckiger, J.; Schmidt, S.; Donzella, V.; Sherwali, A.; Ratner, D.M.; Chrostowski, L.; Cheung, K.C. Sub-wavelength grating for enhanced ring resonator biosensor. *Opt. Express* **2016**, *24*, 15672–15686. [CrossRef] [PubMed]
47. Kirk, J.T.; Fridley, G.E.; Chamberlain, J.W.; Christensen, E.D.; Hochberg, M.; Ratner, D.M. Multiplexed inkjet functionalization of silicon photonic biosensors. *Lab Chip* **2011**, *11*, 1372–1377. [CrossRef] [PubMed]

48. Armani, D.; Min, B.; Martin, A.; Vahala, K.J. Electrical thermo-optic tuning of ultrahigh-Q microtoroid resonators. *Appl. Phys. Lett.* **2004**, *85*, 5439. [CrossRef]
49. Van Laere, F.; Roelkens, G.; Ayre, M.; Schrauwen, J.; Taillaert, D.; Van Thourhout, D.; Krauss, T.F.; Baets, R. Compact and Highly Efficient Grating Couplers between Optical Fiber and Nanophotonic Waveguides. *J. Light. Technol.* **2007**, *25*, 151–156. [CrossRef]
50. Maire, G.; Vivien, L.; Sattler, G.; Kazmierczak, A.; Sanchez, B.; Gylfason, K.B.; Griol, A.; Marris-Morini, D.; Cassan, E.; Giannone, D.; et al. High efficiency silicon nitride surface grating couplers. *Opt. Express* **2008**, *16*, 328–333. [CrossRef] [PubMed]
51. Lukosz, W.; Tiefenthaler, K. Embossing technique for fabricating integrated optical components in hard inorganic waveguiding materials. *Opt. Lett.* **1983**, *8*, 537–539. [CrossRef]
52. Tiefenthaler, K.; Lukosz, W. Sensitivity of grating couplers as integrated-optical chemical sensors. *J. Opt. Soc. Am. B* **1989**, *6*, 209–220. [CrossRef]
53. Vörös, J.; Ramsden, J.; Csúcs, G.; Szendrő, I.; de Paul, S.; Textor, M.; Spencer, N. Optical grating coupler biosensors. *Biomaterials* **2002**, *23*, 3699–3710. [CrossRef]
54. Szendro, I. Art and practice to emboss gratings into sol-gel waveguides. In Proceedings of the Volume 4284, Functional Integration of Opto-Electro-Mechanical Devices and Systems, San Jose, CA, USA, 15 May 2001; Volume 4284, pp. 80–88.
55. Available online: https://www.owls-sensors.com/owls-system (accessed on 3 April 2021).
56. Karasiński, P. Sensor properties of planar waveguide structures with grating couplers. *Opto Electron. Rev.* **2007**, *15*, 168–178. [CrossRef]
57. Karasiński, P. Embossable grating couplers for planar evanescent wave sensors. *Opto Electron. Rev.* **2011**, *19*, 10–21. [CrossRef]
58. Kazmierczak, A.; Slowikowski, M.; Pavlov, K.; Filipiak, M.; Vervaeke, M.; Tyszkiewicz, C.; Ottevaere, H.; Piramidowicz, R.; Karasinski, P. Efficient, low-cost optical coupling mechansim for TiO2-SiO2 sol-gel derived slab waveguide surface grating coupler sensors. *Opt. Appl.* **2020**, *50*, 539–549.
59. Brandenburg, A.; Gombert, A. Grating couplers as chemical sensors: A new optical configuration. *Sens. Actuators B Chem.* **1993**, *17*, 35–40. [CrossRef]
60. Wiki, M.; Gao, H.; Juvet, M.; Kunz, R. Compact integrated optical sensor system. *Biosens. Bioelectron.* **2001**, *16*, 37–45. [CrossRef]
61. Horvath, R.; Pedersen, H.C.; Skivesen, N.; Svanberg, C.; Larsen, N.B. Fabrication of reverse symmetry polymer waveguide sensor chips on nanoporous substrates using dip-floating. *J. Micromech. Microengin.* **2005**, *15*, 1260–1264. [CrossRef]
62. Basu, D.; Sen, K.; Hossain, S.M.; Das, J. Instrumentation and Development of Grating Coupler Sensor for Cost-effective and Precision Measurement of Biomolecules. In Proceedings of the 2019 10th International Conference on Computing, Communication and Networking Technologies (ICCCNT), Kanpur, India, 6–8 July 2019; pp. 1–4.
63. Li, H.-Y.; Hsu, W.-C.; Liu, K.-C.; Chen, Y.-L.; Chau, L.-K.; Hsieh, S.; Hsieh, W.-H. A low cost, label-free biosensor based on a novel double-sided grating waveguide coupler with sub-surface cavities. *Sens. Actuators B Chem.* **2015**, *206*, 371–380. [CrossRef]
64. Xia, M.; Zhang, P.; Qiao, K.; Bai, Y.; Xie, Y.-H. Coupling SPP with LSPR for Enhanced Field Confinement: A Simulation Study. *J. Phys. Chem. C* **2015**, *120*, 527–533. [CrossRef]
65. Wu, F.; Thomas, P.A.; Kravets, V.G.; Arola, H.O.; Soikkeli, M.; Iljin, K.; Kim, G.; Kim, M.; Shin, H.S.; Andreeva, D.V.; et al. Layered material platform for surface plasmon resonance biosensing. *Sci. Rep.* **2019**, *9*, 1–10. [CrossRef]
66. Reinhard, I.; Miller, K.; Diepenheim, G.; Cantrell, K.; Hall, W.P. Nanoparticle Design Rules for Colorimetric Plasmonic Sensors. *ACS Appl. Nano Mater.* **2020**, *3*, 4342–4350. [CrossRef]
67. Mauriz, E. Clinical applications of visual plasmoni colorimetric sensing. *Sensors* **2020**, *20*, 6214. [CrossRef]
68. Bauch, M.; Toma, K.; Toma, M.; Zhang, Q.; Dostalek, J. Plasmon-Enhanced Fluorescence Biosensors: A Review. *Plasmonics* **2014**, *9*, 781–799. [CrossRef] [PubMed]
69. Fossati, S.; Hageneder, S.; Menad, S.; Maillart, E.; Dostalek, J. Multiresonant plasmonic nanostructure for ultrasensitive fluorescence biosensing. *Nanophotonics* **2020**, *9*, 3673–3685. [CrossRef]
70. Langer, J.; Jimenez de Aberasturi, D.; Aizpurua, J.; Alvarez-Puebla, R.A.; Auguie, B.; Baumberg, J.J.; Bazan, G.C.; Bell, S.E.J.; Boisen, A.; Brolo, A.G.; et al. Present and Future of Surface Enhanced Raman Scattering. *ACS Nano* **2020**, *14*, 28–117. [CrossRef]
71. Pilot, R.; Signorini, R.; Durante, C.; Orian, L.; Bhamidipati, M.; Fabris, L. A Review on Surface-Enhanced Raman Scattering. *Biosensors* **2019**, *9*, 57. [CrossRef] [PubMed]
72. Wang, T.; Dong, Z.; Koay, E.H.H.; Yang, J.K.W. Surface-Enhanced Infrared Absorption Spectroscopy Using Charge Transfer Plasmons. *ACS Photon* **2019**, *6*, 1272–1278. [CrossRef]
73. Pereira, C.F.; Viegas, I.M.A.; Sobrinha, I.G.S.; Pereira, G.; Pereira, G.A.D.L.; Krebs, P.; Mizaikoff, B. Surface-enhanced infrared absorption spectroscopy using silver selenide quantum dots. *J. Mater. Chem. C* **2020**, *8*, 10448–10455. [CrossRef]
74. Lin, L. *Manipulation of Near Field Propagation and Far Field Radiation of Surface Plasmon Polariton*; Springer: Singapore, 2017.
75. Tabassum, R.; Mishra, S.K.; Gupta, B.D. Surface plasmon resonance-based fiber optic hydrogen sulphide gas sensor utilizing Cu-ZnO thin films. Phys. *Chem. Chem. Phys.* **2013**, *15*, 11868–11874. [CrossRef]
76. Gupta, B.D.; Verma, R.K. Surface Plasmon Resonance-Based Fiber Optic Sensors: Principle, Probe Designs, and Some Applications. *J. Sens.* **2009**, *2009*, 1–12. [CrossRef]
77. Lu, L.; Jiang, Z.; Hu, Y.; Zhou, H.; Liu, G.; Chen, Y.; Luo, Y.; Chen, Z. A portable optical fiber SPR temperature sensor based on a smart-phone. *Opt. Express* **2019**, *27*, 25420–25427. [CrossRef]
78. Duarte, D.P.; Alberto, N.; Bilro, L.; Nogueira, R. Theoretical Design of a High Sensitivity SPR-Based Optical Fiber Pressure Sensor. *J. Light. Technol.* **2015**, *33*, 4606–4611. [CrossRef]

79. Mi, H.; Wang, Y.; Jin, P.; Lei, L. Design of a ultrahigh-sensitivity SPR-based optical fiber pressure sensor. *Optik* **2013**, *124*, 5248–5250. [CrossRef]
80. Kim, H.-M.; Park, J.-H.; Lee, S.-K. Fabrication and Measurement of Fiber Optic Surface Plasmon Resonance Sensor Based on Polymer Microtip and Gold Nanoparticles Composite. *IEEE Sens. J.* **2020**, *20*, 9895–9900. [CrossRef]
81. Joe, H.-E.; Yun, H.; Jo, S.-H.; Jun, M.B.; Min, B.-K. A review on optical fiber sensors for environmental monitoring. *Int. J. Precis. Eng. Manuf. Technol.* **2018**, *5*, 173–191. [CrossRef]
82. Homola, J. Surface plasmon resonance biosensors for food safety, in Optical Sensors. In *Springer Series on Chemical Sensors and Biosensors (Methods and Applications), vol. 1*; Springer: Berlin/Heidelberg, Germany, 2004.
83. Zeni, L.; Perri, C.; Cennamo, N.; Arcadio, F.; D'Agostino, G.; Salmona, M.; Beeg, M.; Gobbi, M. A portable optical-fibre-based surface plasmon resonance biosensor for the detection of therapeutic antibodies in human serum. *Sci. Rep.* **2020**, *10*, 1–9. [CrossRef]
84. Li, D.; Lu, B.; Zhu, R.; Yu, H.; Xu, K. An optofluidic system with volume measurement and surface plasmon resonance sensor for continuous glucose monitoring. *Biomicrofluidics* **2016**, *10*, 011913. [CrossRef]
85. Zainuddin, N.; Ariannejad, M.; Arasu, P.; Harun, S.; Zakaria, R. Investigation of cladding thicknesses on silver SPR based side-polished optical fiber refractive-index sensor. *Results Phys.* **2019**, *13*, 102255. [CrossRef]
86. Caucheteur, C.; Guo, T.; Albert, J. Review of plasmonic fiber optic biochemical sensors: Improving the limit of detection. *Anal. Bioanal. Chem.* **2015**, *407*, 3883–3897. [CrossRef]
87. Mahmood, A.I.; Ibrahim, R.K.; Mahmood, A.I.; Ibrahim, Z.K. Design and simulation of surface plasmon resonance sensors for environmental monitoring. In *Journal of Physics: Conference Series*; IOP: Bristol, UK, 2018; Volume 1003.
88. Taylor, A.D.; Ladd, J.; Homola, J.; Jiang, S. Surface plasmon resonance (SPR) sensors for the detection of bacterial pathogens. In *Principles of Bacterial Detection:Biosensors, Recognition Receptors and Microsystems*; Springer: New York, NY, USA, 2008; pp. 83–108.
89. Fontana, E.; Dulman, H.; Doggett, D.; Pantell, R. Surface plasmon resonance on a single mode optical fiber. *IEEE Trans. Instrum. Meas.* **1998**, *47*, 168–173. [CrossRef]
90. Mao, P.; Luo, Y.; Chen, X.; Fang, J.; Huang, H.; Chen, C.; Peng, S.; Zhang, J.; Tang, J.; Lu, H.; et al. Design and optimization of multimode fiber sensor based on surface plasmon resonance. In Proceedings of the Numerical Simulation of Optoelectronic Devices, Palma de Mallorca, Spain, 1–4 September 2014; pp. 119–120.
91. Hoseinian, M.S.; Bolorizadeh, M.A. Design and Simulation of a Highly Sensitive SPR Optical Fiber Sensor. *Photon Sens.* **2018**, *9*, 33–42. [CrossRef]
92. Xie, T.; He, Y.; Yang, Y.; Zhang, H.; Xu, Y. Highly Sensitive Surface Plasmon Resonance Sensor Based on Graphene-Coated U-shaped Fiber. *Plasmonics* **2021**, *16*, 205–213. [CrossRef]
93. Verma, R.K.; Gupta, B.D. Theoretical modelling of a bi-dimensional U-shaped surface plasmon resonance based fiber optic sensor for sensitivity enhancement. *J. Phys. D Appl. Phys.* **2008**, *41*, 095106. [CrossRef]
94. Yu, H.; Chong, Y.; Zhang, P.; Ma, J.; Li, D. A D-shaped fiber SPR sensor with a composite nanostructure of MoS2-graphene for glucose detection. *Talanta* **2020**, *219*, 121324. [CrossRef] [PubMed]
95. Arasu, P.T.; Al-Qazwini, Y.; Onn, B.I.; Noor, A.S.M. Fiber Bragg grating based surface plasmon resonance sensor utilizing FDTD for alcohol detection applications. In Proceedings of the 2012 IEEE 3rd International Conference on Photonics, Pulau Pinang, Malaysia, 1–3 October 2012; pp. 93–97.
96. Kim, Y.-C.; Peng, W.; Banerji, S.; Booksh, K.S. Tapered fiber optic surface plasmon resonance sensor for analyses of vapor and liquid phases. *Opt. Lett.* **2005**, *30*, 2218–2220. [CrossRef] [PubMed]
97. Navarrete, M.-C.; Díaz-Herrera, N.; González-Cano, A.; Esteban, Ó. Surface plasmon resonance in the visible region in sensors based on tapered optical fibers. *Sens. Actuators B Chem.* **2014**, *190*, 881–885. [CrossRef]
98. Aray, A.; Chiavaioli, F.; Arjmand, M.; Trono, C.; Tombelli, S.; Giannetti, A.; Cennamo, N.; Soltanolkotabi, M.; Zeni, L.; Baldini, F. SPR-based plastic optical fibre biosensor for the detection of C-reactive protein in serum. *J. Biophotonics* **2016**, *9*, 1077–1084. [CrossRef] [PubMed]
99. Wang, W.; Mai, Z.; Chen, Y.; Wang, J.; Li, L.; Su, Q.; Li, X.; Hong, X. A label-free fiber optic SPR biosensor for specific detection of C-reactive protein. *Sci. Rep.* **2017**, *7*, 1–8. [CrossRef]
100. Tran, D.T.; Knez, K.; Janssen, K.P.; Pollet, J.; Spasic, D.; Lammertyn, J. Selection of aptamers against Ara h 1 protein for FO-SPR biosensing of peanut allergens in food matrices. *Biosens. Bioelectron.* **2013**, *43*, 245–251. [CrossRef]
101. Luo, B.; Yan, Z.; Sun, Z.; Liu, Y.; Zhao, M.; Zhang, L. Biosensor based on excessively titled fiber grating in thin-cladding optical fiber for sensitive and selective detection of low glucose concentration. *Opt. Express* **2015**, *23*, 32429–32440. [CrossRef]
102. Lu, J.; Van Stappen, T.; Spasic, D.; Delport, F.; Vermeire, S.; Gils, A.; Lammertyn, J. Fiber optic-SPR platform for fast and sensitive in fliximab detection in serum of inflammatory bowel disease patients. *Biosens. Bioelectron.* **2016**, *79*, 173–179. [CrossRef]
103. Yeh, P.; Yariv, A.; Marom, E. Theory of Bragg fiber. *J. Opt. Soc. Am.* **1978**, *68*, 1196–1201. [CrossRef]
104. Knight, J.C.; Birks, T.A.; Russell, P.S.J.; Atkin, D.M. All-silica single-mode optical fiber with photonic crystal cladding. *Opt. Lett.* **1996**, *21*, 1547–1549. [CrossRef]
105. Pinto, A.M.R.; Lopez-Amo, M. Photonic Crystal Fibers for Sensing Applications. *J. Sens.* **2012**, *2012*, 1–21. [CrossRef]
106. Kim, J.A.; Hwang, T.; Dugasani, S.R.; Amin, R.; Kulkarni, A.; Park, S.H.; Kim, T. Graphene based fiber optic surface plasmon resonance for bio-chemical sensor applications. *Sens. Actuator B Chem.* **2013**, *187*, 426–433. [CrossRef]

107. Xu, H.; Wu, L.; Dai, X.; Gao, Y.; Xiang, Y. An ultra-high sensitivity surface plasmon resonance sensor based on graphene-aluminum-graphene sandwich-like structure. *J. Appl. Phys.* **2016**, *120*, 053101. [CrossRef]
108. Lin, C.; Chen, S. Design of high-performance Au-Ag-dielectric-graphene based surface plasmon resonance biosensors using genetic algorithm. *J. Appl. Phys.* **2019**, *125*, 113101. [CrossRef]
109. Chen, S.; Lin, C. Sensitivity comparison of graphene based surface plasmon resonance biosensor with Au, Ag and Cu in the visible region. *Mater. Res. Express* **2019**, *6*, 056503. [CrossRef]
110. Shuai, B.; Xia, L.; Liu, D. Coexistence of positive and negative refractive index sensitivity in the liquid-core photonic crystal fiber based plasmonic sensor. *Opt. Express* **2012**, *20*, 25858–25866. [CrossRef] [PubMed]
111. Mollah, A.; Islam, S.R.; Yousufali; Abdulrazak, L.F.; Hossain, M.B.; Amiri, I. Plasmonic temperature sensor using D-shaped photonic crystal fiber. *Results Phys.* **2020**, *16*, 102966. [CrossRef]
112. Chen, N.; Chang, M.; Lu, X.; Zhou, J.; Zhang, X. Numerical Analysis of Midinfrared D-Shaped Photonic-Crystal-Fiber Sensor Based on Surface-Plasmon-Resonance Effect for Environmental Monitoring. *Appl. Sci.* **2020**, *10*, 3897. [CrossRef]
113. Liu, C.; Su, W.; Liu, Q.; Lu, X.; Wang, F.; Sun, T.; Chu, P.K. Symmetrical dual D-shape photonic crystal fibers for surface plasmon resonance sensing. *Opt. Express* **2018**, *26*, 9039–9049. [CrossRef] [PubMed]
114. Chen, Y.; Xie, Q.; Li, X.; Zhou, H.; Hong, X.; Geng, Y. Experimental realization of D-shaped photonic crystal fiber SPR sensor. *J. Phys. D Appl. Phys.* **2017**, *50*, 025101. [CrossRef]
115. Yasli, A.; Ademgil, H.; Haxha, S. D-shaped photonic crystal fiber based surface plasmon resonance sensor. In Proceedings of the 26th Signal Processing and Communications Applications Conference (SIU), Izmir, Turkey, 2–5 May 2018.
116. Lu, Y.; Yang, X.; Wang, M.; Yao, J. Surface plasmon resonance sensor based on hollow-core PCFs filled with silver nanowires. *Electron. Lett.* **2015**, *51*, 1675–1677. [CrossRef]
117. Lu, Y.; Wang, M.; Hao, C.; Zhao, Z.; Yao, J. Temperature sensing using photonic crystal fiber filled with silver nanowires and liquid. *Photonics J. IEEE* **2014**, *6*, 1–7. [CrossRef]
118. Semenova, D.; Gernaey, K.V.; Silina, Y.E. Exploring the potential of electroless and electroplated noble metal-semiconductor hybrids within bio- and environmental sensing. *Analyst* **2018**, *143*, 5646–5669. [CrossRef]
119. Malinsky, P.; Slepicka, P.; Hnatowicz, V.; Svorcik, V. Early stages of growth of gold layers sputter deposited on glass and silicon substrates. *Nanoscale Res. Lett.* **2012**, *7*, 241. [CrossRef]
120. Svorcik, V.; Siegel, J.; Sutta, P.; Mistrik, J.; Janicek, P.; Worsch, P.; Kolska, Z. Annealing of gold nanostructures sputtered on glass substrate. *Appl. Phys. A* **2011**, *102*, 605.
121. Sennett, R.S.; Scott, G.D. The structure of evaporated metal films and their optical properties. *J. Opt. Soc. Am. A Opt. Image Sci. Vis.* **1950**, *40*, 203. [CrossRef]
122. Khurgin, J.B. Replacing noble metals with alternative materials in plasmonics and metamaterials:How good an idea? *Phil. Trans. R. Soc. A* **2017**, *375*, 20160068. [CrossRef]
123. Naik, G.V.; Shalaev, V.M.; Boltasseva, A. Alternative plasmonic materials:beyond gold and silver. *Adv. Mater.* **2013**, *25*, 3264–3294. [CrossRef]
124. Shao, L.; Liu, Z.; Hu, J.; Gunawardena, D.; Tam, H.-Y. Optofluidics in microstructured optical fibers. *Micromachines* **2018**, *9*, 145. [CrossRef] [PubMed]
125. Irawan, R.; Chuan, T.S.; Meng, T.C.; Ming, T.K. Rapid constructions of microstructures for optical fiber sensors using a commercial CO2 laser system. *Open Biomed. Eng. J.* **2008**, *2*, 28–35. [CrossRef] [PubMed]
126. Argyros, A. Microstructures in polymer fibers for optical fibres, THz waveguides, and fibre-based metamaterials. *Int. Sch. Res. Not.* **2013**, *2013*, 785162.
127. Rindorf, L.; Hoiby, P.E.; Jensen, J.B.; Pedersen, L.H.; Bang, O.; Geschke, O. Towards biochips using microstructured optical fiber sensors. *Anal. Bioanal. Chem.* **2006**, *385*, 1370–1375. [CrossRef] [PubMed]
128. Lu, H.; Wang, G.; Liu, X. Manipulation of light in MIM plasmonic waveguide systems. *Chin. Sci. Bull.* **2013**, *58*, 3607–3616. [CrossRef]
129. Hu, H.; Zeng, X.; Wang, L.; Xu, Y.; Song, G.; Gan, Q. Surface plasmon coupling efficiency from nanoslit apertures to metal-insulator-metal waveguides. *Appl. Phys. Lett.* **2012**, *101*, 121112. [CrossRef]
130. Butt, M.A.; Khonina, S.N.; Kazanskiy, N.L. Ultra-short lossless plasmonic power splitter design based on metal-insulator-metal waveguide. *Laser Phys.* **2019**, *30*, 016201. [CrossRef]
131. Hill, M.T.; Marell, M.; Leong, E.; Smalbrugge, B.; Zhu, Y.; Sun, M.; van Veldhoven, P.J.; Geluk, E.J.; Karouta, F.; Oei, Y.-S.; et al. Lasing in metal-insulator-metal sub-wavelength plasmonic waveguides. *Opt. Express* **2009**, *17*, 11107–11112. [CrossRef]
132. Yu, Y.; Si, J.; Ning, Y.; Sun, M.; Deng, X. Plasmonic wavelength splitter based on a metal-insulator-metal waveguide with a graded grating coupler. *Opt. Lett.* **2017**, *42*, 187–190. [CrossRef]
133. Khani, S.; Danaie, M.; Rezaei, P. Siza reduction of MIM surface plasmon based optical bandpass filters by the introduction of arrays of silver nano-rods. *Phys. E Low Dimens. Syst. Nanostruct.* **2019**, *113*, 25–34. [CrossRef]
134. Butt, M.A. Numerical investigation of a small footprint plasmonic Bragg grating structure with a high extinction ratio. *Photon. Lett. Pol.* **2020**, *12*, 82–84. [CrossRef]
135. Butt, M.A.; Khonina, S.N.; Kazanskiy, N.L. An array of nano-dots loaded MIM square ring resonator with enhanced sensitivity at NIR wavelength range. *Optik* **2020**, *202*, 163655. [CrossRef]

136. Butt, M.A.A.; Kazanskiy, N. Enhancing the sensitivity of a standard plasmonic MIM square ring resonator by incorporating the Nano-dots in the cavity. *Photon. Lett. Pol.* **2020**, *12*, 1–3. [CrossRef]
137. Butt, M.A.; Khonina, S.N.; Kazanskiy, N.L. Metal-insulator-metal nano square ring resonator for gas sensing applications. *Waves Random Complex Media* **2021**, *31*, 146–156. [CrossRef]
138. A Butt, M.; Kazanskiy, N.L.; Khonina, S.N. Nanodots decorated asymmetric metal–insulator–metal waveguide resonator structure based on Fano resonances for refractive index sensing application. *Laser Phys.* **2020**, *30*, 076204. [CrossRef]
139. Butt, M.A.; Khonina, S.N.; Kazanskiy, N.L. A plasmonic colour filter and refractive index sensor applications based on metal-insulator-metal square micro-ring cavities. *Laser Phys.* **2020**, *30*, 016205. [CrossRef]
140. Butt, M.A.; Kazanskiy, N.L.; Khonina, S.N. Highly Sensitive Refractive Index Sensor Based on Plasmonic Bow Tie Configuration. *Photon. Sens.* **2020**, *10*, 223–232. [CrossRef]
141. Butt, M.A.; Khonina, S.N.; Kazanskiy, N.L. Plasmonic refractive index sensor based on M-I-M square ring resonator. In Proceedings of the International Conference on Computing, Electronic and Electrical Engineering (ICE Cube), Quetta, Pakistan, 12–13 November 2018.
142. Barizuddin, S.; Bok, S.; Gangopadhyay, S. Plasmonic sensors for disease detection-A review. *Nanomed. Nanotechnol.* **2016**, *7*, 1000373.
143. A Butt, M.; Khonina, S.N.; Kazanskiy, N.L. A multichannel metallic dual nano-wall square split-ring resonator: Design analysis and applications. *Laser Phys. Lett.* **2019**, *16*, 126201. [CrossRef]
144. Behnam, M.A.; Emami, F.; Sobhani, Z.; Koohi-Hosseinabadi, O.; Dehghanian, A.R.; Zebarjad, S.M.; Moghim, M.H.; Oryan, A. Novel Combination of Silver Nanoparticles and Carbon Nanotubes for Plasmonic Photo Thermal Therapy in Melanoma Cancer Model. *Adv. Pharm. Bull.* **2018**, *8*, 49–55. [CrossRef]
145. Sagor, R.H.; Hassan, F.; Sharmin, S.; Adry, T.Z.; Emon, A.R. Numerical investigation of an optimized plasmonic on-chip refractive index sensor for temperature and blood group detection. *Results Phys.* **2020**, *19*, 103611. [CrossRef]
146. Rakhshani, M.R. Optical refractive index sensor with two plasmonic double-square resonators for simultaneous sensing of human blood groups. *Photon. Nanostruct. Fundam. Appl.* **2020**, *39*, 100768. [CrossRef]
147. Nejat, M.; Nozhat, N. Multi-band MIM refractive index biosensor based on Ag-air grating with equivalent circuit and T-matrix methods in near-infrared region. *Sci. Rep.* **2020**, *10*, 1–12. [CrossRef]
148. Rakhshani, M.R. Refractive index sensor based on concentric triple racetrack resonators side-coupled to metal–insulator–metal waveguide for glucose sensing. *J. Opt. Soc. Am. B* **2019**, *36*, 2834–2842. [CrossRef]
149. Liu, D.; Wang, J.; Zhang, F.; Pan, Y.; Lu, J.; Ni, X. Tunable Plasmonic Band-Pass Filter with Dual Side-Coupled Circular Ring Resonators. *Sensors* **2017**, *17*, 585. [CrossRef] [PubMed]
150. Rahmatiyar, M.; Afsahi, M. Design of a refractive index plasmonic sensor based on a ring resonator coupled to a MIM waveguide containing tapered defects. *Plasmonics* **2020**, *15*, 2169–2176. [CrossRef]
151. Jankovic, N.; Cselyuszka, N. Multiple Fano-like MIM plasmonic structure based on triangular resonator for refractive index sensing. *Sensors* **2018**, *18*, 287.
152. Chau, Y.F.C.; Chao, C.T.C.; Huang, H.J.; Kumara, N.; Lim, C.M.; Chiang, H.P. Ultra-high refractive index sensing structure based on a metal-insulator-metal waveguide-coupled T-shaped cavity with metal nanorod defects. *Nanomaterials* **2019**, *9*, 1433.
153. Kamada, S.; Okamoto, T.; El-Zohary, S.E.; Haraguchi, M. Design optimization and fabrication of Mach-Zehnder interferometer based on MIM plasmonic waveguides. *Opt. Express* **2016**, *24*, 16224–16231. [CrossRef]
154. Butt, M.A.; Kazanskiy, N.L. Nanoblocks embedded in L-shaped nanocavity of a plasmonic sensor for best sensor performance. *Opt. Appl.* **2021**, *51*, 109–120.
155. Cao, J.; Sun, T.; Grattan, K.T. Gold nanorod-based localized surface plasmon resonance biosensors:a review. *Sens. Actuators B Chem.* **2014**, *195*, 332–351. [CrossRef]
156. Masson, J.F.; Live, L.S.; Murray-Methot, M.P. Nanohole arrays in chemical analysis:manufacturing methods and applications. *Analyst* **2010**, *135*, 1483–1489. [CrossRef]
157. Kazanskiy, N.L.; Butt, M.A.; Degtyarev, S.A.; Khonina, S.N. Achievements in the development of plasmonic waveguide sensors for measuring the refractive index. *Comput. Opt.* **2020**, *44*, 295–318. [CrossRef]
158. Kazanskiy, N.L.; Khonina, S.N.; Butt, M.A. Plasmonic sensors based on Metal-insulator-Metal waveguides for refractive index sensing applications: A brief review. *Phys. E* **2020**, *117*, 113798. [CrossRef]
159. Veselago, V.G. Experimental demonstration of negative index of refraction. *Sov. Phys. Usp.* **1968**, *10*, 509.
160. Pendry, J.B.; Holden, A.J.; Stewart, W.J.; Youngs, I. Extremely low frequency plasmons in metallic mesostructures. *Phys. Rev. Lett.* **1996**, *76*, 4773–4776. [CrossRef]
161. Smith, D.R.; Padilla, W.J.; Vier, D.C.; Nemat-Nasser, S.C.; Schultz, S. Composite medium with simultaneously negative permeability and permittivity. *Phys. Rev. Lett.* **2000**, *84*, 4184–4187. [CrossRef]
162. Cen, C.; Chen, Z.; Xu, D.; Jiang, L.; Chen, X.; Yi, Z.; Wu, P.; Li, G.; Yi, Y. High quality factor, high sensitivity metamaterial graphene-perfect absorber based on critical coupling theory and impedance matching. *Nanomaterials* **2020**, *10*, 95. [CrossRef]
163. Butt, M.A.; Kazanskiy, N.L. Narrowband perfect metasurface absorber based on impedance matching. *Photonics Lett. Poland* **2020**, *12*, 88–90. [CrossRef]
164. Wu, Z.; Kelp, G.; Yogeesh, M.N.; Li, W.; McNicholas, K.M.; Briggs, A.; Rajeeva, B.B.; Akinwande, D.; Bank, S.R.; Shvets, G.; et al. Dual-band moire metasurface patches for multifunctional biomedical applications. *Nanoscale* **2016**, *8*, 18461–18468. [CrossRef]

165. Kazanskiy, N.L.; Butt, M.A.; Khonina, S.N. Carbon dioxide gas sensor based on polyhexamethylene biguanide polymer deposited on silicon nano-cylinders metasurface. *Sensors* **2021**, *21*, 378. [CrossRef]
166. Meinzer, N.; Barnes, W.L.; Hooper, I.R. Plasmonic meta-atoms and metasurfaces. *Nat. Photonics* **2014**, *8*, 889–898. [CrossRef]
167. Ding, J.; Xu, N.; Ren, H.; Lin, Y.; Zhang, W.; Zhang, H. Dual-wavelength terahertz metasurfaces with independent phase and amplitude control at each wavelength. *Sci. Rep.* **2016**, *6*, 34020. [CrossRef]
168. Ahmadivand, A.; Gerislioglu, B.; Manickam, P.; Kaushik, A.; Bhansali, S.; Nair, M.; Pala, N. Rapid detection of infectious envelope proteins by magnetoplasmonic toroidal metasensors. *ACS Sens.* **2017**, *2*, 1359–1368. [CrossRef] [PubMed]
169. Yesilkoy, F.; Arvelo, E.R.; Jahani, Y.; Liu, M.; Tittl, A.; Cevher, V.; Kivshar, Y.; Altug, H. Ultrasensitive hyperspectral imaging and biodetection enabled by dielectric metasurfaces. *Nat. Photonics* **2019**, *13*, 390–396. [CrossRef]
170. Zhang, S.; Wong, C.L.; Zeng, S.; Bi, R.; Tai, K.; Dholakia, K.; Olivo, M. Metasurfaces for biomedical applications:imaging and sensing from a nanophotonics perspective. *Nanophotonics* **2020**, *10*, 259–293. [CrossRef]
171. Serita, K.; Murakami, H.; Kawayama, I.; Tonouchi, M. A terahertz-microfluidic chip with a few arrays of asymmetric meta-atoms for the ultra-trace sensing of solutions. *Photonics* **2019**, *6*, 12. [CrossRef]
172. Rodionov, S.A.; Remnev, M.A.; Klimov, V.V. Refractive index sensor based on all-dielectric gradient metasurface. *Sens. Bio Sens. Res.* **2019**, *22*, 100263. [CrossRef]
173. Pahlevaninezhad, H.; Khorasaninejad, M.; Huang, Y.W.; Shi, Z.; Hariri, L.P.; Adams, D.C.; Ding, V.; Zhu, A.; Qiu, C.W.; Capasso, F.; et al. Nano-optic endoscope for high-resolution optical coherence tomography in vivo. *Nat. Photonics* **2018**, *12*, 540–547. [CrossRef]
174. Chen, W.T.; Zhu, A.Y.; Capasso, F. Flat optics with dispersion-engineered metasurfaces. *Nat. Rev. Mater.* **2020**, *5*, 604–620. [CrossRef]
175. Yu, N.; Capasso, F. Flat optics with designer metasurfaces. *Nat. Mater.* **2014**, *13*, 139–150. [CrossRef]
176. Wu, P.C. Flat optics with nanophotonic metasurface. In *JSAP-OSA Joint Symposia*; OSA Publisher: Hokkaido, Japan, 2019.
177. Lee, D.; Gwak, J.; Badloe, T.; Palomba, S.; Rho, J. Metasurfaces-based imaging and applications:from miniaturized optical components to functional imaging platforms. *Nanoscale Adv.* **2020**, *2*, 605–625. [CrossRef]
178. Sung, J.; Lee, G.Y.; Lee, B. Progresses in the practical metasurface for holography and lens. *Nanophotonics* **2019**, *8*, 1701–1718. [CrossRef]
179. Wang, Y.; Ali, M.A.; Chow, E.C.; Dong, L.; Lu, M. An optofluidic metasurface for lateral flow-through detection of breast cancer biomarker. *Biosens. Bioelectron.* **2018**, *107*, 224–229. [CrossRef]
180. Geng, Z.; Zhang, X.; Fan, Z.; Lv, X.; Chen, H. A route to terahertz metamaterial biosensor integrated with microfluidics for liver cancer biomarker testing in early stage. *Sci. Rep.* **2017**, *7*, 16378. [CrossRef] [PubMed]
181. Yan, X.; Yang, M.; Zhang, Z.; Liang, L.; Wei, D.; Wang, M.; Zhang, M.; Wang, T.; Liu, L.; Xie, J.; et al. The terahertz electromagnetically induced transparency-like metamaterials for sensitive biosensors in the detection of cancer cells. *Biosens. Bioelectron.* **2019**, *126*, 485–492. [CrossRef] [PubMed]
182. Wang, Y.; Zhao, C.; Wang, J.; Luo, X.; Xie, L.; Zhan, S.; Kim, J.; Wang, X.; Liu, X.; Ying, Y. Wearable plasmonic-metasurface sensor for noninvasive and universal molecular fingerprint detection on biointerfaces. *Sci. Adv.* **2021**, *7*, eabe4553.
183. Lorwongtragool, P.; Sowade, E.; Watthanawisuth, N.; Baumann, R.R.; Kerdcharoen, T. A novel wearable electronic nose for healthcare based on flexible printed chemical sensor array. *Sensors* **2014**, *14*, 19700–19712. [CrossRef] [PubMed]
184. Zhan, Z.; Lin, R.; Tran, V.-T.; An, J.; Wei, Y.; Du, H.; Tran, T.; Lu, W. Paper/carbon nanotube-based wearable pressure sensor for physiological signal acquisition and soft robotic skin. *ACS Appl. Mater. Interfaces* **2017**, *9*, 37921–37928. [CrossRef]
185. Chaghamirzaei, P.; Raeyani, D.; Khosravi, A.; Allahveisi, S.; Abdollahi-Kai, B.; Bayat, F.; Olyaeefar, B.; Ahmadi-Kandjani, S. Real-time detection of gas and chemical vapor flows by silica inverse-opals. *IEEE Sens. J.* **2019**, *19*, 7961–7967. [CrossRef]
186. Pakchin, P.S.; Fathi, M.; Ghanbari, H.; Saber, R.; Omidi, Y. A novel electrochemical immunosensor for ultrasensitive detection of CA125 in ovarian cancer. *Biosens. Bioelectron.* **2020**, *153*, 112029.
187. Xia, L.; Song, J.; Xu, R.; Liu, D.; Dong, B.; Xu, L.; Song, H. Zinc oxide inverse opal electrodes modified by glucose oxidase for electrochemical and photoelectrochemical biosensor. *Biosens. Bioelectron.* **2014**, *59*, 350–357. [CrossRef] [PubMed]
188. Yablonovitch, E. Inhibited spontaneous emission in solid-state physics and electronics. *Phys. Rev. Lett.* **1987**, *58*, 2059. [CrossRef] [PubMed]
189. John, S. Strong localization of photons in certain disordered dielectric superlattices. *Phys. Rev. Lett.* **1987**, *58*, 2486. [CrossRef]
190. Zhang, Y.; Li, B. Photonic crystal-based bending waveguides for optical interconnections. *Opt. Express* **2006**, *14*, 5723–5732. [CrossRef] [PubMed]
191. Butt, M.A.; Khonina, S.N.; Kazanskiy, N.L. 2D-Photonic crystal heterostructures for the realization of compact photonic devices. *Photon. Nanostruct. Fundam. Appl.* **2021**, *44*, 100903. [CrossRef]
192. Butt, M.A.; Kazanskiy, N.L. Two-dimensional photonic crystal heterostructure for light steering and TM-polarization maintaining applications. *Laser Phys.* **2021**, *31*, 036201. [CrossRef]
193. Liu, B.; Liu, Y.F.; Jia, C.; He, X.D. All-optical diode structure based on asymmetrical coupling by a micro-cavity and FP cavity at two sides of photonic crystal waveguide. *AIP Adv.* **2016**, *6*, 065316. [CrossRef]
194. Notomi, M. Negative refraction in photonic crystals. *Opt. Quantum Electron.* **2002**, *34*, 133–143. [CrossRef]
195. Noori, M.; Soroosh, M.; Baghban, H. Self-Collimation in Photonic Crystals: Applications and Opportunities. *Ann. Der Phys.* **2018**, *530*, 1700049. [CrossRef]

196. Nishijima, Y.; Ueno, K.; Juodkazis, S.; Mizeikis, V.; Misawa, H.; Tanimura, T.; Maeda, K. Inverse silica opal photonic crystals for optical sensing applications. *Opt. Express* **2007**, *15*, 12979–12988. [CrossRef] [PubMed]
197. Cunningham, B.; Zhang, M.; Zhuo, Y.; Kwon, L.; Race, C. Review of recent advances in biosensing with photonic crystals. *IEEE Sens. J.* **2014**, *16*, 3349–3366. [CrossRef] [PubMed]
198. Rodriguez, G.A.; Markov, P.; Cartwright, A.P.; Choudhury, M.H.; Afzal, F.O.; Cao, T.; Halimi, S.I.; Retterer, S.T.; Kravchenko, I.I.; Weiss, S.M. Photonic crystal nanobeam biosensors based on porous silicon. *Opt. Express* **2019**, *27*, 9536–9549. [CrossRef]
199. Fathi, F.; Rashidi, M.R.; Pakchin, P.S.; Ahmadi-Kandjani, S.; Nikniazi, A. Photonic crystal based biosensors: Emerging inverse opals for biomarker detection. *Talanta* **2021**, *221*, 121615. [CrossRef] [PubMed]
200. Lee, W.S.; Kang, T.; Kim, S.H.; Jeong, J. An antibody-immobilized silica inverse opal nanostructure for label-free optical biosensors. *Sensors* **2018**, *18*, 307. [CrossRef] [PubMed]
201. Li, J.; Zhao, X.; Wei, H.; Gu, Z.Z.; Lu, Z. Macroporous ordered titanium dioxide (TiO2) inverse opal as a new label-free immunosensor. *Anal. Chim. Acta* **2008**, *625*, 63–69. [CrossRef]
202. Shen, W.; Li, M.; Wang, B.; Liu, J.; Li, Z.; Jiang, L.; Song, Y. Hierarchical optical antenna: Gold nanoparticle-modified photonic crystal for highly-sensitive label free DNA detection. In *J. Mater. Chem.*; 2012; Volume 22, pp. 8127–8133.
203. Feng, X.; Xu, J.; Liu, Y.; Zhao, W. Visual sensors of an inverse opal hydrogel for the colorimetric detection of glucose. *J. Mater. Chem. B* **2019**, *7*, 3576–3581. [CrossRef]
204. Zhao, X.; Xue, J.; Mu, Z.; Huang, Y.; Lu, M.; Gu, Z. Gold nanoparticle incorporated inverse opal photonic crystal capillaries for optofluidic surface enhanced Raman spectroscopy. *Biosens. Bioelectron.* **2015**, *72*, 268–274. [CrossRef]
205. Jiang, Y.; Liu, D.; Yang, Y.; Xu, R.; Zhang, T.; Sheng, K.; Song, H. Photoelectrochemical detection of alpha-fetoprotein based on ZnO inverse opals structure electrodes modified by Ag_2S nanoparticles. *Sci. Rep.* **2016**, *6*, 38400. [CrossRef] [PubMed]
206. Choi, E.; Choi, Y.; Nejad, Y.H.; Shin, K.; Park, J. Label-free specific detection of immunoglobulin G antibody using nanoporous hydrogel photonic crystals. *Sens. Actuators B Chem.* **2013**, *180*, 107–113. [CrossRef]
207. Inci, F.; Tokel, O.; Wang, S.; Gurkan, U.A.; Tasoglu, S.; Kuritzkes, D.R.; Demirci, U. Nanoplasmonic quantitative detection of intact viruses from unprocessed whole blood. *ACS Nano* **2013**, *7*, 4733–4745. [CrossRef] [PubMed]
208. Shafiee, H.; Jahangir, M.; Inci, F.; Wang, S.; Willenbrecht, R.B.M.; Giguel, F.F.; Tsibris, A.M.N.; Kuritzkes, D.R.; Demirci, U. Acute On-Chip HIV Detection Through Label-Free Electrical Sensing of Viral Nano-Lysate. *Small* **2013**, *9*, 2553–2563. [CrossRef]
209. Shamah, S.M.; Cunningham, B.T. Label-free cell-based assays using photonic crystal optical biosensors. *Analyst* **2011**, *136*, 12. [CrossRef]
210. Endo, T.; Ozawa, S.; Okuda, N.; Yanagida, Y.; Tanaka, S.; Hatsuzawa, T. Reflectometric detection of influenza virus in human saliva using nanoimprint lithography-based flexible two-dimensional photonic crystal biosensor. *Sens. Actuator B Chem.* **2010**, *148*, 269–276. [CrossRef]
211. Shafiee, H.; Lidstone, E.A.; Jahangir, M.; Inci, F.; Hanhauser, E.; Henrich, T.J.; Kuritzkes, D.R.; Cunningham, B.T.; Demirci, U. Nanostructured Optical Photonic Crystal Biosensor for HIV Viral Load Measurement. *Sci. Rep.* **2014**, *4*, 4116. [CrossRef]
212. Holzgrafe, J.; Sinclair, N.; Zhu, D.; Shams-Ansari, A.; Colangelo, M.; Hu, Y.; Zhang, M.; Berggren, K.K.; Loncar, M. Cavity electro-optics in thin-film lithium niobate for efficient microwave-to-optical transduction. *Optica* **2020**, *7*, 1714–1720. [CrossRef]
213. Chang, M.S.; Burlamacchi, P.; Hu, C.; Whinnery, J.R. Light amplification in a thin film. *Appl. Phys. Lett.* **1972**, *20*, 313.
214. Nikoleli, G.P.; Nikolelis, D.P.; Siontorou, C.G.; Nikolelis, M.T.; Karapetis, S. The application of lipid membranes in biosensing. *Membranes* **2018**, *8*, 108. [CrossRef]
215. Nikoleli, G.P.; Nikolelis, D.P.; Siontorou, C.G.; Karapetis, S.; Nikolelis, M.T. Application of biosensors based on lipid membranes for the rapid detection of toxins. *Biosensors* **2018**, *8*, 61. [CrossRef] [PubMed]
216. Mueller, P.; Rudin, D.O. Action potentials induced in biomolecular lipid membranes. *Nature* **1968**, *217*, 713. [CrossRef]
217. Sugawara, M.; Kojima, K.; Sazawa, H.; Umezawa, Y. Ion-channel sensors. *Anal Chem.* **1987**, *59*, 2842–2846. [CrossRef]
218. Holden, M.A.; Needham, D.; Bayley, H. Functional biometworks from nanoliter water droplets. *J. Am. Chem. Soc.* **2007**, *129*, 8650–8655. [CrossRef]
219. Zhong, X.B.; Reynolds, R.; Kidd, J.R.; Kidd, K.K.; Jenison, R.; Marlar, R.A.; Ward, D.C. Single-nucleotide polymorphism genotyping on optical thin-film biosensor chips. *Proc. Natl. Acad. Sci. USA* **2003**, *100*, 11559–11564. [CrossRef]
220. Ceylan, K.H.; Kulah, H.; Ozgen, C. Thin film biosensors. In *Thin Films and Coatings in Biology. Biological and Medical Physics, Biomedical Engineering*; Springer: Dordrecht, The Netherlands, 2013.
221. Sasaki, T.; Kasai, H.; Nishibori, E. Tightly binding valence electron in aluminum observed through X-ray charge density study. *Sci. Rep.* **2018**, *8*, 11964. [CrossRef]
222. Tseng, M.L.; Yang, J.; Semmlinger, M.; Zhang, C.; Nordlander, P.; Halas, N.J. Two-dimensional active tuning of an aluminum plasmonic array for full-spectrum response. *Nano Lett.* **2017**, *17*, 6034–6039. [CrossRef] [PubMed]
223. Lambert, A.S.; Valiulis, S.N.; Malinick, A.S.; Tanabe, I.; Cheng, Q. Plasmonic biosensing with aluminum thin films under the Kretschmann configuration. *Anal. Chem.* **2020**, *92*, 8654–8659. [CrossRef] [PubMed]
224. Handoyo, T.; Kondoh, J. Development of gold thin-film for optical-based biosensor. In *AIP Conference Proceedings*; AIP Publishing: College Park, MD, USA, 2020; Volume 2230, p. 020008.
225. Iftimie, N.; Savin, A.; Steigmann, R.; Faktorova, D.; Salaoru, I. ZnO thin film as MSG for sensitive biosensor. *IOP Conf. Ser. Mater. Sci. Eng.* **2016**, *145*, 042030. [CrossRef]

226. Moirangthem, R.S.; Chang, Y.C.; Wei, P.K. Ellipsometry study on gold-nanoparticle-coated gold thin film for biosensing application. *Biomed. Opt. Express* **2011**, *2*, 2569. [CrossRef]
227. Zhao, Y.; Tong, R.J.; Xia, F.; Peng, Y. Current status of optical fiber biosensor based on surface plasmon resonance. *Biosens. Bioelectron.* **2019**, *142*, 111505. [CrossRef]
228. Jang, H.S.; Park, K.N.; Kim, J.P.; Sim, S.J.; Kwon, O.J.; Han, Y.G.; Lee, K.S. Sensitive DNA biosensor based on a long-period grating formed on the side-polished fiber surface. *Opt. Express* **2009**, *17*, 3855–3860. [CrossRef] [PubMed]
229. Chiavaioli, F.; Baldini, F.; Tombelli, S.; Trono, C.; Giannetti, A. Biosensing with optical fiber gratings. *Nanophotonics* **2017**, *6*, 663–679. [CrossRef]
230. Coelho, L.; Almeida, J.; Santos, J.L.; Jorge, P.; Martins, M.C.; Viegas, D.; Queiros, R.B. Aptamer-based fiber sensor for thrombin detection. *J. Biomed. Opt.* **2016**, *21*, 87005. [CrossRef] [PubMed]
231. Shevchenko, Y.; Francis, T.J.; Blair, D.A.; Walsh, R.; DeRosa, M.C.; Albert, J. In Situ Biosensing with a surface plasmon resonance fiber grating aptasensor. *Anal. Chem.* **2011**, *83*, 7027–7034. [CrossRef] [PubMed]
232. Liu, M.; Li, J.; Li, B.X. A colorimetric aptamer biosensor based on cationic polythiophene derivative as peroxidase mimetics for the ultrasensitive detection of thrombin. *Talanta* **2017**, *175*, 224–228. [CrossRef]
233. Li, S.; Zhang, D.; Zhang, Q.; Lu, Y.L.; Li, N.; Chen, Q.W.; Liu, Q.J. Electrophoresis-enhanced localized surface plasmon resonance sensing based on nanocup array for thrombin detection. *Sens. Actuators B Chem.* **2016**, *232*, 219–225. [CrossRef]
234. Villatoro, J.; Monzon-Hernandez, D. Low-cost optical fiber refractive-index sensor based on core diameter mismatch. *J. Light. Technol.* **2006**, *24*, 1409–1413. [CrossRef]
235. Owji, E.; Mokhtari, H.; Ostovari, F.; Darazereshki, B.; Shakiba, N. 2D materials coated on etched optical fibers as humidity sensor. *Sci. Rep.* **2021**, *11*, 1771. [CrossRef] [PubMed]
236. Komanec, M.; Nemecek, T.; Vidner, P.M.; Martan, T.; Lahodny, F.; Zvanovec, S. Structurally-modified tapered optical fiber sensors for long-term detection of liquids. *Opt. Fiber Technol.* **2019**, *47*, 187–191. [CrossRef]
237. Asseh, A.; Sandgren, S.; Ahlfeldt, H.; Sahlgren, B.; Stubbe, R.; Edwall, G. Fiber optical Bragg grating refractometer. *Fiber Integr. Opt.* **1998**, *17*, 51–62.
238. Ladicicco, A.; Cusano, A.; Campopiano, S.; Cutolo, A.; Giordano, M. Thinned fiber Bragg gratings as refractive index sensors. *IEEE Sens. J.* **2005**, *5*, 1288–1295. [CrossRef]
239. Chryssis, A.N.; Saini, S.S.; Lee, S.M.; Yi, H.; Bentley, W.E.; Dagenais, M. Detecting hybridization of DNA by highly sensitive evanescent field etched core fiber Bragg grating sensors. *IEEE J. Sel. Top. Quantum Electron.* **2005**, *11*, 864. [CrossRef]
240. Guo, T.; Liu, F.; Liu, Y.; Chen, N.K.; Guan, B.O.; Albert, J. In-situ detection of density alteration in non-physiological cells with polarimetric tilted fiber grating sensors. *Biosens. Bioelectron.* **2014**, *55*, 452–458. [CrossRef] [PubMed]